UNIVERSITÀ DEGLI STUDI DI TRIESTE

XXXI CICLO DEL DOTTORATO DI RICERCA IN INGEGNERIA ED ARCHITETTURA

ESTIMATION OF LTE SIGNALS' TIME OF ARRIVAL IN A MULTI-BAND ENVIRONMENT

Settore scientifico-disciplinare: **ING-INF/03 - TELECOMUNICAZIONI**

DOTTORANDO
MATTEO NOSCHESE

COORDINATORE
PROF. DIEGO MICHELI

SUPERVISORE DI TESI
PROF. FULVIO BABICH

CO-SUPERVISORE DI TESI
DOTT. CHRIS MARSHALL

ANNO ACCADEMICO 2017/2018

What you complainin' about? he thought. ****** be carryin' you, playa.*

Skin

Enormity by W.G. Marshall

Abstract

This thesis summarizes the research work done on the estimation of the Time of Arrival (ToA) of signals in Orthogonal Frequency Division Multiplexing (OFDM)-based communication systems. The estimated ToA values may be employed for positioning purposes in land-based networks, thus providing an alternative means of localization to satellite-based technologies. By employing signals of opportunity (SoP), this information can be obtained without the need to allocate transmission resources specifically for positioning purposes.

The OFDM multiplexing technique is widely employed in modern telecommunication standards and presents interesting properties with regard to ToA estimation. In particular, the Third Generation Partnership Project (3GPP) Long Term Evolution is interesting for its diffusion, geographical coverage, and wide transmission bandwidth, making it a prime candidate for research. The upcoming fifth generation (5G) mobile systems are also expected to employ an OFDM-based physical layer, leading to further possibilities of application and development.

In the first part of the work, novel algorithms for the estimation of ToA in OFDM-based systems have been developed. The Slope-based algorithm exploits the phase rotation of sub-carriers induced by the channel to obtain the estimation with simple unwrap and linear fitting operations. It can be shown that if the Direct Path (DP) is also the stronger one, the ToA can be inferred from slope of the phase rotation even when secondary paths are present. A piecewise variant with outliers removal is also introduced to reduce the effects of noise and phase jumps on the final estimation.

The Difference-Based algorithm (DBTE) instead relies on a rough first estimate of the channel parameters to obtain an estimation of the first prop-

agation path delay even when secondary paths present, on average, larger amplitudes than the direct one. Multiple consecutive OFDM symbols can be aggregated to achieve a more accurate and reliable estimate. The DBTE method achieves good performance at the cost of a greater computational complexity than the slope-based method.

In the second part of the research work, the use of multiple OFDM signals transmitted on separate frequency bands has been explored. The developed research is based on the assumption that the propagation environment is highly correlated between the transmission bands, which is reasonable if the carrier frequencies are relatively close to each other. This allows one to make full use of the higher bandwidth occupied by the set of signals as a whole, rather than just the bandwidth of each signal on its own, to achieve improved precision and multi-path robustness.

The Space-Alternating Generalized Expectation-Maximization (SAGE) algorithm has been chosen for the task, because of its versatility and good performance in complex propagation environments. SAGE presents the advantage of being applicable to multi-band scenarios without the need of significant modifications to its basic formulation. A simulator has been implemented in Matlab to evaluate the possible benefits of dual-band usage, showing significant performance gain even when the two signals are not perfectly synchronized.

In the LTE network multiple transmitters may be allocated on the same physical base station mast, in order to decrease deployment costs and improve the network coverage and quality of service. A set of live measurements on downlink LTE signals has been performed in Monfalcone, Italy. The considered cellular mast carries 3 cell IDs for each operator and transmits on LTE band 20. The Cell-Specific Reference Signal (CRS) has been used as

the reference signal of choice. The CRS is always transmitted, allowing it to be used in a fully opportunistic way. The Time of Arrival is derived from the gathered data, showing (in agreement with simulations) that the combination of signals from multiple bands leads to a reduced range and standard deviation in the estimations.

While the focus of this thesis is ToA estimation in OFDM-based environments, the research on Low-Density Parity Check (LDPC) channel codes started with the master thesis has been continued out as a side activity. The research explored the generation of puncturation patterns for LDPC codes through the use of a cost function based on the code's own node degree distribution. The performance bound for LDPC codes proposed by Richardson and Urbanke has been investigated as well, proposing an approximation of the bound that is confirmed by simulations.

Acknowledgements

The first and foremost acknowledgement for this work goes to my supervisors, Professor Fulvio Babich of University of Trieste and Dr. Chris Marshall of u-blox. Without their initiative my PhD would never have taken place. Their support has been steady and it has been crucial throughout the path of my studies. There have been times of disagreement and misunderstandings, but never have I been let down by my supervisors, and for that I cannot thank them enough.

I wouldn't have gone far without the amazing place that is my family. Each of them deserves a lot more than the few lines I'm writing here.

To my father Vincenzo, for giving his incredible support to me and to everyone else. He really shows me what it means to be dedicated.

To my mother Orietta, for always taking care of me and loving me with more than just words.

To my sister Chiara, because no one fills your life as much as a sibling does. She gives me a lot more than what I give her.

To my grandmother Lina, for loving me the way only a grandma can.

To my grandfather Livio, who is no longer with us. No one has ever believed in me as much as he did, and I miss him dearly.

I want to thank my friends for the moments we have lived together, for accepting me and, why not, for coping with me at times. More often than not, they have had a higher opinion of me than I do, helping me feel better about myself. Without them all my life would be not only lonelier, but also a lot emptier.

I would like to give the people who helped me with my PhD the mention they deserve: the u-blox guys, especially Andrea Dalla Torre and my predecessor Marco Driusso, and fellow PhD student Alessandro Pin in Udine.

They have always been competent and friendly and they lent me their support every time I needed without a second thought.

In my time at the Microonde lab I had the chance to spend time with the people of the Telecommunications group: Max, Giulia, Alessandro and Francesca. Getting to know all of them has been amazing, and they really bring our humble lab to life. I would also like to remember Prof. Vescovo, whose sudden passing has left a big void in our hearts.

As a PhD student I had the amazing chance to assist younger students with their own thesis activities. Working with them has been a pleasant and enriching experience for me, and I hope for them as well.

For the long hours spent together between silly frolics and more serious topics, once again I want to say thanks to Julia Medina and Nicolai Black.

And once again, the last thank goes to every person to ever attend or work at the Malignani 2000 Technical Institute in Cervignano del Friuli, Italy. To me, simply the best place in the world.

Summary

The Ph.D. work presented in this dissertation was developed as part of a collaboration between the Department of Engineering and Architecture of the University of Trieste and the company u-blox, and has been fully funded by the latter. During the three years of the doctoral program, this work has been supported by u-blox U.K. Ltd through the figure of Dr. Chris Marshall and u-blox Italy s.p.a. through its Sgonico branch.

Positioning and navigation technologies have been experiencing a massive increase in popularity over the past few years, and are now commonly available to a large number of end users. The extent of applications spans from military, security, and disaster relief purposes to vehicle navigation, fleet management and tracking of shipped goods, to simple entertainment. The rising sector of autonomous robots and self-driving vehicles also requires precise and robust positioning to offer reliable services and ensure the safety of people. Recently, a more network-oriented approach to positioning is gaining attention [1, 2]. In network localization, the position of nodes inside the network becomes an integral part of networking. As such, efficient and reliable positioning methods are needed to implement the localization function.

The positioning task is most often performed by means of a satellite positioning system (GNSS, Global Navigation Satellite System) such as the Global Positioning System (GPS). GNSS-enabled modules have become affordable to a vast number of users and are found in a majority of mobile devices such as smartphones and tablets. However, the accuracy of the position estimated via GNSS is often subject to many impairments that may negatively impact on the quality of the location service, or may even completely disrupt it. Indoor, subterranean, and urban canyon environments can degrade the reception of the positioning signal, leading to a failure of the

service. Furthermore, adding a dedicated GNSS-enabled module to a device increases its complexity, which, in turn, leads to higher production costs and increased power consumption. These two drawbacks are highly undesirable on mobile devices. Alternative methods able to provide an accurate positioning for land-based systems become hence necessary. Various ranging and positioning algorithms have been developed for this purpose, and the topic has been widely explored in the literature [3]. These methods are based on the estimation of a number of wave parameters for each propagation path, such as its complex amplitude, Time of Arrival (ToA), Doppler shift, and Angle of Arrival, or on differential parameter estimation [4, 5]. Among those techniques, those based on ToA estimation account for a significant portion.

The thesis is structured as follows.

Chapter 1 introduces the problem of positioning exploiting OFDM signals, with a specific focus on LTE downlink signals.

The principles of the OFDM transmission technique are laid out, to give a better understanding of the properties of OFDM transmission, especially those regarding the estimation of the ToA. The OFDM system model is extended to a more general multi-band notation that is used as a reference throughout the research work. The OFDM technique is widely employed in modern wide-band communication standards thanks to its efficiency and simple FFT-based implementation, making it a prime candidate for research [6]. Another advantage of OFDM is the easy exploitation of pilot tones in an opportunistic way. In fact, the use of Signals of Opportunity (SoP) for ranging and positioning purposes presents many advantages [7, 8].

The 3GPP-LTE standard is a communication system of particular interest because of its wide geographic coverage, signal strength and signal bandwidth. It employs the OFDM technique for its downlink layer. Hence,

an introductory overview of the LTE standard is then given, with a focus on its downlink layer and the reference signals that have been exploited throughout the research work. Those signals are employed opportunistically, thus without the need to allocate resources specifically for the purpose of positioning. For this reason, several methods have been developed that exploit the LTE framework for positioning [9, 10, 11, 12].

Finally, a classification of existing positioning techniques is presented. Modern positioning methods may be subdivided in different categories based on the nature of the measured quantity, the area of coverage, or the employed technology.

Chapter 2 describes the novel algorithms that were developed for Time or Arrival estimation in OFDM systems. The estimation of the ToA is a widely researched topic, and ToA-based positioning systems are the vast majority among those used nowadays. Novel positioning and navigation techniques such as cooperative positioning [13, 14, 15] often employ ToA-based ranging, furthering the need for efficient, accurate estimation algorithms that can be implemented on mobile devices with low power and transmission resources.

The OFDM technique presents interesting properties in that regard [16, 17], thanks to the subdivision of the total bandwidth in a large number of narrow-band channels. The Slope-Based algorithm exploits the sub-carriers phase rotation, which presents a linear behavior, to obtain an estimation of the ToA through a least-squares linear fitting procedure. The measured sub-carrier phase rotation undergoes an unwrapping process. It is crucial to avoid spurious jumps in the unwrapped phase at this may lead to an estimation bias. When the Direct Path (DP) is also the stronger one, the first path ToA can be inferred from the slope of the phase rotation even when secondary paths are presents. A piecewise variant with outliers removal is also intro-

duced to reduce the effects of noise and phase jumps on the final estimation. Piecewise linear fitting proves especially beneficial when the Signal to Noise ratio is low. The Slope-Based method achieves good performance when the direct path propagation is dominant, while retaining a low computational complexity.

The Difference-Based ToA Estimation algorithm (DBTE) instead relies on a rough first estimate of the propagation channel parameters with a simple FFT-based method. Using the inferred values, an estimation of the first propagation path delay is obtained even when secondary paths present, on average, larger amplitudes than the direct one. Multiple consecutive symbols can be aggregated to achieve a more accurate and reliable estimate. The DBTE method achieves good performance at the cost of a greater computational complexity than the Slope-Based method.

Chapter 3 treats the topic of multi-band estimation. in some cases, the same information may be sent over multiple frequency bands, so as to give rise to a frequency diversity scenario. The possibility of adopting multiple bands, which requires the availability of wide or redundant bandwidth, might occur, for example, in Gigabit-WiFi networks or in forthcoming 5G systems, thanks to the exploitation of the millimeter-wave domain [18]. In the LTE network, multiple transmitters can be allocated on the same physical base station mast in order to decrease deployment costs and improve the network coverage and quality of service, thus giving rise to a scenario where multiple OFDM signals originate from the same location. This potential invites investigation of the behavior of positioning methods when multiple bands are used. The SAGE algorithm has been chosen for the task because of its versatility and good performance in complex propagation environments, without the need to change its basic mathematical formulation. Firstly introduced as an

extension of Expectation-Maximization (EM), SAGE is a reduced complexity method for the evaluation of the Maximum Likelihood (ML) estimation. More precisely, in SAGE, the multi-dimensional ML estimation problem is subdivided into a certain number of smaller problems to jointly estimate the desired parameters in an iterative way. However, the general lack of synchronization between the clocks of the transmitters allocated on the same physical rack means that additional processing is needed before the information from the two sub-bands can be combined. To this end, two methods are introduced: Signal Combining and Signal Aggregating. These methods aim to achieve better precision by exploiting the additional bandwidth, under the assumption that the propagation environment is flat across the total bandwidth.

Chapter 4 summarizes the numerical results derived from simulations. To validate the novel SAGE-based methods, a simulator has been developed that implements the LTE downlink layer accurately. The obtained gain in performance is assessed choosing the range (difference between the largest and smallest value of a set) and standard deviation as metrics of comparison. Signal Aggregating presents a greater robustness when the propagation environment differs between the considered transmission bands. Signal Combining on the other hand presents a lower computational complexity thanks to the smaller size of the input data.

In the next part of the research, a measurement campaign has been carried out, with the aim to gather data from real LTE base stations. Chapter 5 gives an overview of the instrumentation and tools employed for the measurements, as well as the scenario where the LTE data were gathered. A transmission mast carrying multiple transmitters has been searched for and considered, to observe a multiple transmission bands scenario. A suitable

LTE base station has been located in Monfalcone, Italy. A set of static measures has been performed in several positions around the base station. The gathered data have been processed to extract the basic cell configuration and then the CFR, which is used as input for the estimation algorithm.

Chapter 6 shows the experimental results obtained from real-life LTE signals gathered during the measurement campaign. The methods proposed for band-combining are applied to the data, showing a significant gain with regards to the considered metrics. In agreement with the simulation, the Signal Aggregating method presents a better performance gain than Signal Combining. Both methods are shown to outperform regular single-band estimation.

Finally, Chapter 7 summarizes the most important conclusions and the possible future development.

Contents

1 Introduction

In this chapter the principles at the basis of the research work are laid out.

First, the model for an OFDM communication system and its principles of operation are formally introduced. The classical model for an OFDM communication system is extended to include a multi-band treatise.

The 3GPP LTE cellular standard is then introduced, starting with a general overview. A specific focus is reserved to the OFDM-based downlink physical layer and the reference signals exploited throughout this work to obtain the required estimations.

In the last section, an overview of positioning systems and techniques is given, as well as the criteria used in their classification. Positioning techniques that are based on distance measurements (and thus on Time of Arrival estimation) are explained in greater detail.

1.1 Multi-band OFDM model

The Orthogonal Frequency Division Multiplexing (OFDM) modulation is a technique widely used in wireless communications. It allows high-rate, reliable transmissions in dispersive propagation environments such as the wireless channel, while maintaining a low implementation complexity. As such, many modern communication standards adopt OFDM-based physical layers, such the IEEE 802.11 Wireless Fidelity (Wi-Fi), the 3GPP Long Term Evolution, and the terrestrial Digital Video Broadcasting (DVB) and Digital Audio Broadcasting (DAB).

The basic principle behind OFDM is the same as Frequency Division Multiplexing (FDM), where multiple parallel streams are transmitted separately in the frequency domain, subdividing the available bandwidth in a number of adjacent sub-bands. Thanks to the low data rate and narrow bandwidth of each stream distortion is avoided, because each sub-band can be treated as a narrow-band flat channel even if the overall channel present frequency-selective characteristics.

In OFDM, the streams are transmitted orthogonally to avoid inter-symbol interference [19, 20]. A prominent advantage of OFDM over FDM is the low-complexity generation of the overall transmitted signal. OFDM employs a Discrete Fourier Transform (DFT) based method for baseband signal generation, as opposed to multi-carrier signal generation needed for FDM implementation, where each stream requires its own modulator and demodulator.

In this work, the OFDM model is extended to a multi-band model.

The modeled multi-band OFDM system operates by transmitting the modulated symbols on multiple sub-bands in a parallel way (Fig. 1.1). It is organized as the union of $M \geq 1$ single-band OFDM systems, where the band available to each sub-system is subdivided into a certain number of

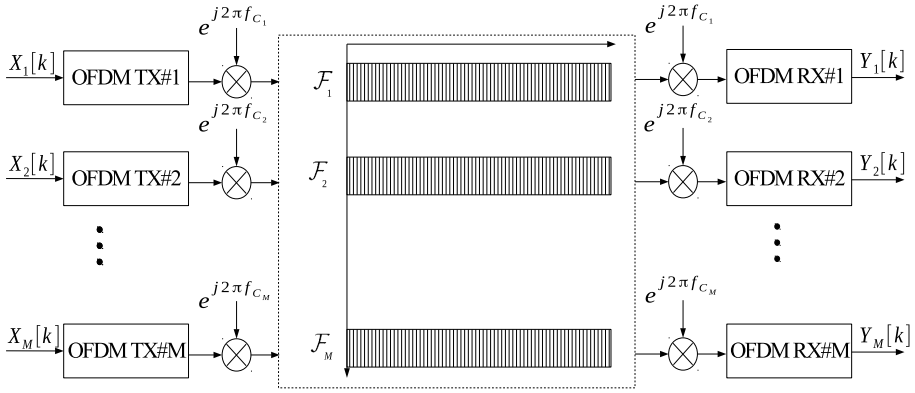

Figure 1.1: Block scheme of a multi-band OFDM system.

single-carrier narrow-band channels. According to the conventional OFDM structure, the single-band sub-carriers are spaced by a frequency $\Delta f = 1/T_s$, where T_s is the duration of an OFDM symbol. It is assumed that the sub-carrier frequency spacing Δf is common to all the sub-systems, and that the bands do not overlap with each other.

The set of sub-carrier frequencies employed by the generic m-th sub-system can be expressed as:

$$\mathcal{F}_m = \{f_{mn} \colon n = 0, \ldots, N_m - 1\}, \quad m = 1, \ldots, M \tag{1.1}$$

where f_{mn} is its n-th sub-carrier frequency and N_m is its number of sub-carriers. Using (1.1), the total set of sub-carrier frequencies may be defined as the union of the sub-carriers' sets of all sub-systems as:

$$\mathcal{F} = \bigcup_{m=1}^{M} \mathcal{F}_m \tag{1.2}$$

The cardinality of $\mathcal{F}$ is $N = \mathcal{C}(\mathcal{F}) = \sum_{m=1}^{M} N_m$, hence the total set of sub-carrier frequencies can also be expressed as:

$$\mathcal{F} = \{f_q \colon q = 1, \ldots, N\} \tag{1.3}$$

Note that, using this general formulation, the frequency spacing between two adjacent sub-carriers is no longer equal to Δf in all cases. Yet, $f_{q+1} - f_q$ remains identical to Δf just if f_{q+1} and f_q belong to the same band. Moreover, observe that the multi-band OFDM system is organized so that $\max[\mathcal{F}_m] \leq \min[\mathcal{F}_{m+1}]$ for $m = 1, \ldots, M-1$, thus the bands are increasingly ordered.

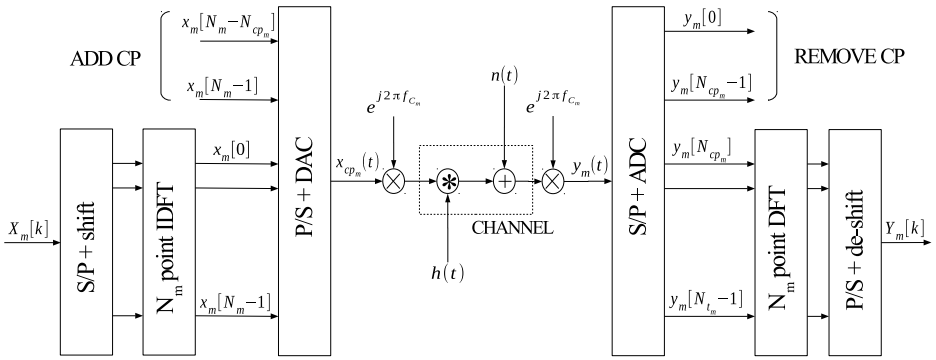

Figure 1.2: Block scheme of the m-th OFDM sub-system.

The structure of the generic single-band OFDM sub-system is shown in Fig. 1.2. The transmitted signal $X_m[k]$ for $m = 1, \ldots, M$ consists of complex symbols taken from the constellation of a digital modulation. This signal can therefore be represented as:

$$X_m[k] = \left[X_m \left[-\frac{N_m}{2} \right], \ldots, X_m \left[\frac{N_m}{2} - 1 \right] \right]^T \tag{1.4}$$

where $(\cdot)^T$ is the transpose operator. $X_m[k]$ is also referred to as OFDM symbol. Accordingly, the OFDM signal can be defined as:

$$x_m(t) = \sum_{k \in \mathcal{K}_m} g(t) X_m[k] e^{j2\pi k \Delta f \cdot t}, \quad t \in [0, T_s[\tag{1.5}$$

where j is the imaginary unit, $\mathcal{K}_m = \{-N_m/2, \ldots, N_m/2 - 1\}$ is the set of the sub-carrier indexes, and $g(t)$ is the shaping impulse, which is assumed,

for simplicity, as an ideal rectangle of amplitude 1 and duration T_s. The discrete time signal $x_m[n]$, sampled with a period $T_m = T_s/N_m$, can then be written as:

$$x_m[n] = x_m(t)\big|_{t=nT_m} = N_m \cdot \mathrm{IDFT}\{\tilde{X}_m[k]\} \qquad n = 0, \ldots, N_m - 1 \tag{1.6}$$

where IDFT denotes the Inverse Discrete Fourier Transform, and $\tilde{X}_m[k]$ is obtained from $X_m[k]$ with the left and right halves swapped. A cyclic prefix is subsequently added to $x_m[n]$ by repeating the N_{cp_m} tail samples of $x_m[n]$ before the sequence, in order to enable the subsequent operation of circular convolution. Therefore, defining $N_{\mathrm{t}_m} = N_m + N_{\mathrm{cp}_m}$, the generated sequence may be represented as:

$$x_{\mathrm{cp}_m}[n] = \begin{cases} x_m[N_m - N_{\mathrm{cp}_m} + n] & n = 0, \ldots, N_{\mathrm{cp}_m} - 1 \\ \\ x_m[n - N_{\mathrm{cp}_m}] & n = N_{\mathrm{cp}_m}, \ldots, N_{\mathrm{t}_m} - 1 \end{cases} \tag{1.7}$$

which, after digital-to-analog conversion at sampling time T_m, provides the continuous-time transmitted signal $x_{\mathrm{cp}_m}(t)$. The signal then undergoes up-conversion at carrier frequency f_{c_m} before it is transmitted on the channel.

After transmission, the OFDM signal experiences the effects of the propagation environment. This element is identified as an L-paths channel, which is modeled by the impulse response:

$$h(t) = \sum_{l=1}^{L} \alpha_l \delta(t - \tau_l) e^{j2\pi f_{D,l}} c(\phi_l) \tag{1.8}$$

where α_l, τ_l, $f_{D,l}$ and $c(\phi_l)$ are, respectively, the complex amplitude, the delay, the Doppler frequency shift and the steering vector of the receiver antenna array, with Angle of Arrival of the l-th path (assumed constant across the duration T_s), and $\delta(t)$ is the Dirac delta function. Now consider the special

case of a single receiver antenna ($c(\phi) = 1$, $\forall\phi$) and slow-moving receiver ($f_{D,l} = 0$, $l = 1, \ldots, L$). The channel impulse response becomes:

$$h(t) = \sum_{l=1}^{L} \alpha_l \delta(t - \tau_l) \tag{1.9}$$

Assuming perfect timing and synchronization at the receiver, it is possible to ignore the effect of up-conversion and down-conversion, and consider the equivalent baseband representation of the OFDM system. Hence, using (1.9), the received signal can be represented as:

$$\begin{aligned} y_m(t) &= h(t) * x_{\mathrm{cp}_m}(t) + n(t) \\ &= \sum_{l=1}^{L} \alpha_l x_{\mathrm{cp}_m}(t - \tau_l) + n(t) \end{aligned} \tag{1.10}$$

where '$*$' denotes the convolution operation and $n(t)$ is the Additive White Gaussian Noise (AWGN). By sampling $y_m(t)$ with a period T_m and applying the DFT operator, one obtains the OFDM-demodulated signal:

$$\begin{aligned} Y_m[k] &= \mathrm{DFT}\left\{ y_m(t) \,|_{t=nT_m} \right\} \\ &= N_m \cdot H_m[k] \tilde{X}_m[k] + \tilde{n}_m[k], \quad k \in \mathcal{K}_m \end{aligned} \tag{1.11}$$

where $\tilde{n}_m[k] = \mathrm{DFT}\left\{ n(t) \,|_{t=nT_m} \right\}$ and $H_m[k]$ is the Channel Frequency Response (CFR), which is evaluated by the Least-Square (LS) estimation:

$$\hat{H}_m[k] = \frac{Y_m[k]}{\tilde{X}_m[k]}, \quad k \in \mathcal{K}_m \tag{1.12}$$

More complex and accurate estimators have been developed [19, 21, 22]. These estimations are used as input for ToA estimation algorithms. Thanks to the subdivision of the available bandwidth, OFDM systems are well suited to obtain CFR samples at several frequencies without performing a frequency sweep and without the need of dedicated hardware.

1.2 The 3GPP Long Term Evolution

The Third Generation Partnership Project (3GPP) Long Term Evolution (LTE) is the global standard for the fourth generation cellular mobile communication systems. It is sometimes referred to as simply LTE or 4G, however the latter denomination is improper as it does not have the characteristics of a true 4G system as defined by 3GPP.

Unlike previous generations systems, the LTE network operates fully in packet switching (IP) mode, with the aim to unify the technology regardless of the service required. LTE offers high data rates, up to 300 Mbps in downlink and 75 Mbps in uplink [23], a latency time of 10 ms, and wide user mobility thanks to various improvements in the core network and radio interface. It also implements Multiple Input Multiple Output (MIMO) and beam-forming techniques to achieve greater user separation and data rates.

1.2.1 The LTE downlink physical layer

The LTE downlink physical layer is based upon the OFDM technique, previously described in Section 1.1. A LTE Base Station (BS) is referred to as eNodeB, and mobile terminals are referred to as User Equipments (UEs). An eNodeB provides its services to many UEs through the use of an Orthogonal Frequency Division Multiple Access (OFDMA) [23] scheme. This allows for a high spectral efficiency, up to 15 bit/s/Hz, and flexible use of the available bandwidth.

The LTE downlink physical layer has two possible configurations, the Frequency Domain Duplexing (FDD) or Type 1 physical layer and the Time Division Duplexing (TDD) or Type 2 physical layer. The Type 1 physical layer is by far the most commonly used: as such, it has been considered throughout the research work. The real-life measurements of Section 5 also

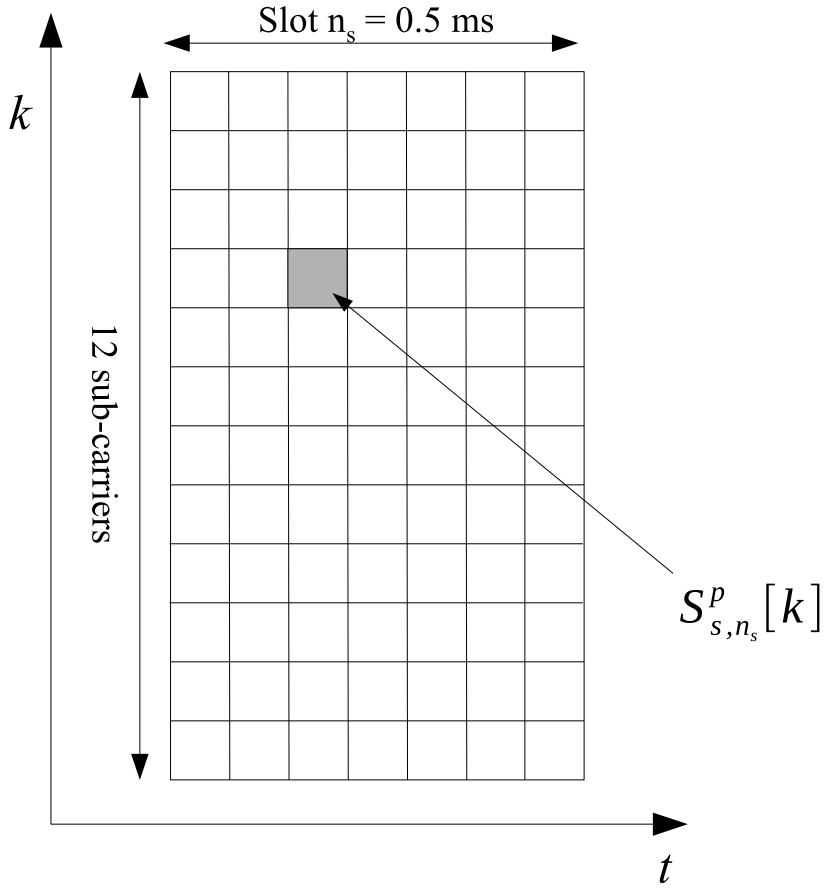

Figure 1.3: Representation of a Resource Block with the time-frequency grid structure. Each square in the grid corresponds to a Resource Element.

refer to an eNodeB with a Type 1 configuration.

When the Type 1 configuration is adopted, the smallest unit of transmission resource corresponds to a single sub-carrier k of an OFDM symbol n, and is referred to as Resource Element (RE). REs are grouped in Resource Blocks (RB), each consisting of $N_{\text{sc}}^{\text{RB}}$ adjacent sub-carriers for the duration of one slot, which is equal to 0.5 ms. RBs can be represented in a time-frequency grid structure, where REs are arranged in a square in the grid and

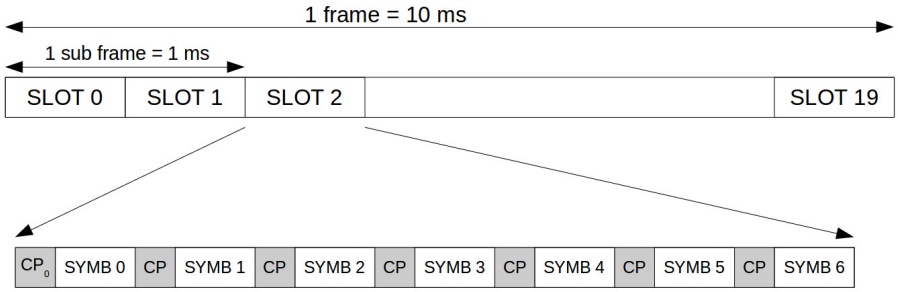

Figure 1.4: Type 1 LTE downlink physical layer configuration with normal CP.

can be uniquely identified by its sub-carrier index k, its slot number n_s, its symbol number n and its antenna port p. The time-frequency grid is depicted in Fig. 1.3.

Each slot is composed of $N_{\text{symb}}^{\text{DL}}$ consecutive OFDM symbols, and each symbol consists of $N_{\text{sc}} = N_{\text{sc}}^{\text{RB}} N_{\text{RB}}^{\text{DL}}$ sub-carriers in the frequency domain, spaced by $\Delta f = 15$ kHz. The number of total sub-carriers used in each OFDM symbol depends on the number $N_{\text{RB}}^{\text{DL}}$ of RBs per slot and, ultimately, on the total signal bandwidth. Table 1.1 lists the possible bandwidth configurations for LTE downlink. Two slots comprise a sub-frame, and 10 sub-frames comprise a radio frame. Hence, a LTE frame consists of 20 slots and has a duration of 10 ms. Fig. 1.4 shows the structure of a LTE downlink frame.

Each OFDM symbol is composed by the actual symbol that carries information, with a duration of $T_s = 1/\Delta f \simeq 66.7\ \mu s$, and the symbol's own cyclic prefix. The LTE sampling time T is defined as $T = T_s/2048 \simeq 32.55\ ns$.

Two different kinds the cyclic prefix are possible: the normal and extended configuration. When the normal CP configuration is adopted $N_{\text{symb}}^{\text{DL}} = 7$, and the CP for the first OFDM symbol of each slot has a duration of $160T$. The following symbols of a slot have a CP with a duration of $144T$ instead.

The normal CP configuration is the most commonly used and has been observed in the real-life measurements as well. The extended CP configuration is usually employed in large rural-area cells where larger delay spread values are supported [23]. Throughout this work, the normal CP configuration is always assumed unless otherwise noted.

1.2.2 LTE Physical Cell ID

Each cell in the LTE network is characterized by a numeric ID $N_{\mathrm{ID}}^{\mathrm{cell}}$, whose value can range between 0 and 503. These values, also referred to as Physical Cell Identities (PCI) are grouped into 168 Physical Cell Identity Groups (PCIG) each containing 3 identities. A PCI is defined as $N_{\mathrm{ID}}^{\mathrm{cell}} = 3N_{\mathrm{ID}}^{(1)} + N_{\mathrm{ID}}^{(2)}$, where $N_{\mathrm{ID}}^{(1)} \in \{0, \ldots, 167\}$ is the PCIG and $N_{\mathrm{ID}}^{(2)} \in \{0, 1, 2\}$ identifies a specific cell within the PCIG. The three identities of a group are assigned to the cells under the control of the same eNodeB. Often, the three cell IDs are assigned to cells deployed to the same base station mast in a sectored configuration. The reference signals of cells belonging to the same PCIG are structured to be orthogonal in the frequency domain (thus easily separable) to avoid overlapping.

Sectors controlled by the same eNodeB are physically separated by means of directional antennas. However, near the edge of a sector or in the presence of reflection, it is still possible for an UE to receive from more than one cell sector. Because the LTE standard specifies a unitary reuse factor, it is possible to exploit the simultaneous reception from multiple cells. This is also possible when the UE is located on the cell edge.

Often, mobile network operators deploy their LTE base stations using the same frequency band for all the sectors. Real-life observations has confirmed this trend, and the BS considered for the measurements adopts this

BW	1.4MHz	3MHz	5MHz	10MHz	15MHz	20MHz
$N_{\mathrm{RB}}^{\mathrm{DL}}$	6	15	25	50	75	100
N_{tot}	12	30	50	100	150	200
N_{sc}	72	180	300	600	900	1200

Table 1.1: List of possible LTE downlink bandwidths.

kind of configuration for the cells belonging to both operators. The unitary frequency reuse factor however leads to a strong Inter Cell Interference (ICI), which needs to be addressed by adopting Inter Cell Interference Coordination (ICIC) techniques.

1.2.3 The Positioning Reference Signal

The LTE standard includes a downlink pilot signal specifically designed for range measurement, the Positioning Reference Signal (PRS). The PRS allows for the acquisition of multiple simultaneous range measurements [24].

The PRS is defined as a QPSK-modulated Gold sequence of length 31. It is transmitted from the antenna port $p = 6$. The mapping of the PRS to REs differs depending on the PCI of the transmitting cell. The mapping presents a frequency-domain shift of $k_s = mod(N_{\mathrm{ID}}^{\mathrm{cell}}, 6)$ sub-carriers. This way, up to six orthogonal PRS signals can be transmitted from cell sectors having six consecutive cell IDs. An example of PRS mapping is depicted in Fig 1.5.

The PRS is designed to span the whole available bandwidth, with one pilot tone every six sub-carriers. The PRS frequency spacing is hence $\Delta f_{\mathrm{PRS}} = 6\Delta f = 90$ kHz and the number of pilot tones per symbol is $N_{\mathrm{sc}}/6$. It is transmitted on specific positioning sub-frames that do not carry user data.

However, most often network operators avoid transmitting the PRS in

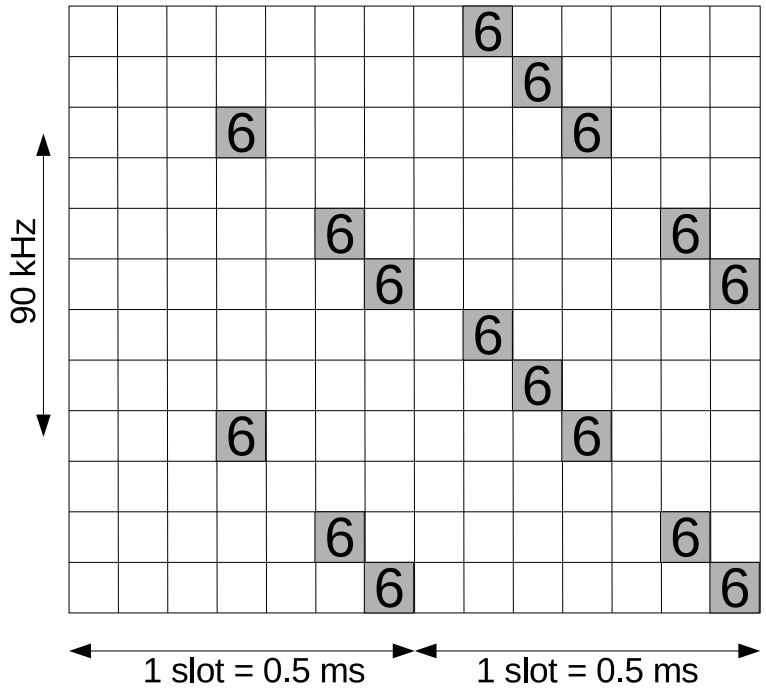

Figure 1.5: PRS mapping to Resource Elements over two consecutive slots. The number in the highlighted squares identifies the antenna port $p = 6$. Note the diagonal mapping spanning the whole available bandwidth.

order to reserve more bandwidth for user data. Hence, this work considers the use of another reference signal, the Cell-Specific Reference Signal (CRS) for the purpose of ToA estimation instead.

1.2.4 The Cell-Specific Reference Signal

The CRS is designed to allow channel estimation and coherent demodulation at the receiver, and it is always transmitted by the base station. Thanks to its characteristics, the CRS can be exploited opportunistically for positioning when the PRS is not present. The CRS is also defined as a QPSK-modulated length-31 Gold sequence, mapped to the REs in a diamond pattern. As in

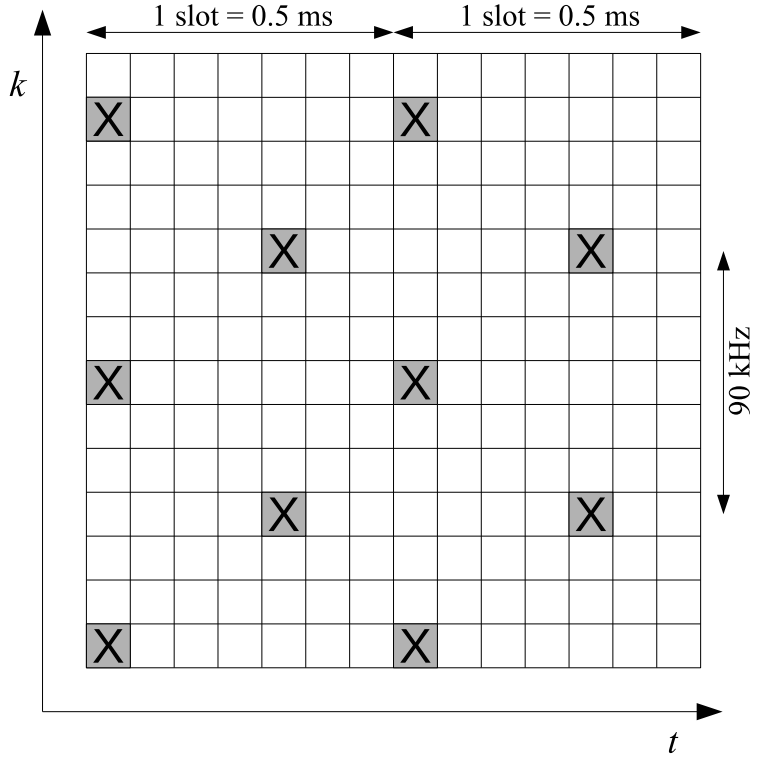

Figure 1.6: CRS mapping to Resource Elements over two consecutive slots. Note the diamond pattern.

the case of the PRS, the mapping of the CRS tones depends on the PCI of the transmitting cell, with a frequency-domain shift of $k_s = mod(N_{\mathrm{ID}}^{\mathrm{cell}}, 6)$ sub-carriers. Six distinct CRS mappings are hence possible. The CRS is transmitted twice per slot, at the symbols $s = 0$ and $s = 4$. When the BS is configured to transmit from more than one antenna port, the CRS tones transmitted from each antenna port are different to avoid overlapping. The CRS pilot tones are mapped to one sub-carrier every six: as such, the number of transmitted CRS tones is $N_{\mathrm{crs}} = N_{\mathrm{sc}}/6$ and the spacing between them is $\Delta f_{\mathrm{CRS}} = 6\Delta f = 90$ kHz. The LTE standard specifies the mapping of the CRS to REs based on the Physical Cell ID ($PCI \in \{0, \ldots, 503\}$). Fig. 1.6

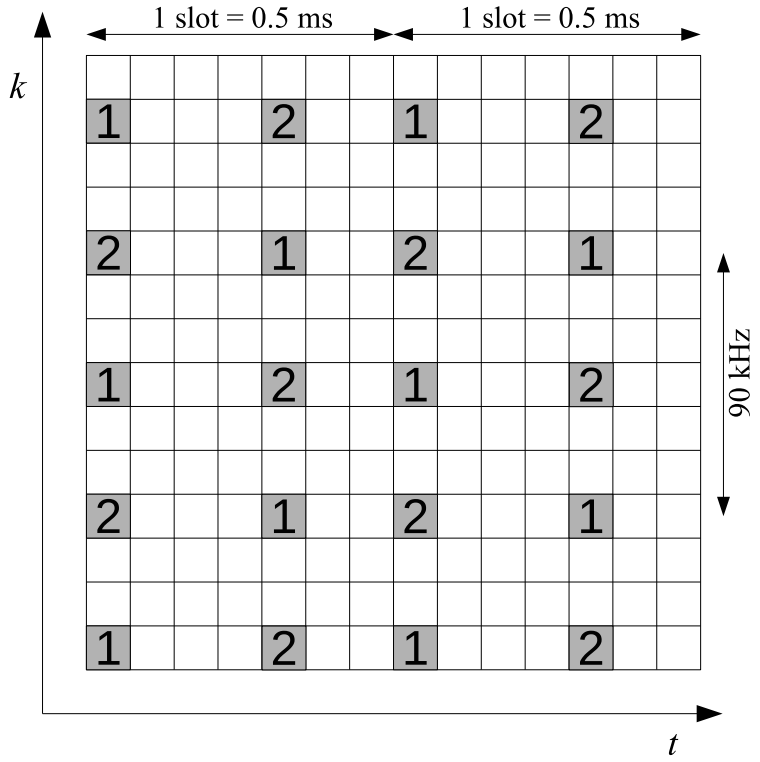

Figure 1.7: CRS mapping to Resource Elements over two consecutive slots when the 2 antenna ports configuration is employed. The numbers in the highlighted squares identify the antenna port.

shows a possible mapping of the CRS when transmitted from a single antenna port. When the configuration with 2 antenna ports is adopted, the CRS pilot symbols are transmitted as shown in Fig. 1.7.

1.3 Positioning

Over the last decades a wide number of different positioning systems have been developed, exploiting many different techniques and algorithm to achieve localization of mobile stations [25]. These methods are most often based on the measurement of the properties of a wireless signal [26].

The positioning systems most commonly employed are the Global Navigation Satellite Systems (GNSSs), including the Global Positioning System (GPS) [27] as well as Europe's Galileo, the Russian GLONASS, the Chinese BeiDou and many others. Such systems exploit distance measurements from the satellites of a low orbit constellation. By estimating the Time of Arrival of the satellite signals, terminals on the ground are enabled to determine their position on a worldwide scale. Localization-related services are in fact widely employed, ranging from military and security application to fleet management, navigation, and entertaining. GNSS-enabled modules have become affordable and are thus found in the majority of commercially available mobile devices. Phones, tablets, and other mobile devices commonly include a GNSS-enable module.

However, the accuracy of the position estimated via GNSS is often subject to many impairments that could negatively impact on the quality of the localization service, or may even completely disrupt it. Indoor, subterranean, and urban canyon environments could degrade the reception of the positioning signal, leading to a failure of the service. Furthermore, adding a dedicated GNSS-enabled module to a device increases its complexity, which, in turn, leads to higher production costs and increased power consumption. These two drawbacks are highly undesirable on mobile devices.

Alternative methods able to provide an accurate positioning become hence necessary. Land-based systems can be employed to assist GNSS-based posi-

tioning when its performance falters or even to replace it altogether as the sole providers of the service. Mobile cellular networks in particular enjoy vast diffusion and a comprehensive geographic coverage, making them prime candidates for land-based positioning purposes. The 3GPP LTE mobile system includes an integrated positioning framework [24] based on the PRS, which as already noted in Section 1.2.3 sees only a limited use nowadays. Other frameworks have been developed for smaller-scale positioning using wireless LAN or sensors networks signals to perform positioning, especially for short-range localization [28, 29].

1.3.1 Structure of a positioning system

Regardless of the type of system and the specifications, the base elements of a wireless or terrestrial positioning system are referred to as nodes. Nodes can be subdivided in two broad categories: agents and anchors.

- Agents are the nodes to be located and as such have unknown positions. In cellular-based systems, the agents correspond to the mobile terminals.

- Anchors nodes have known and usually fixed locations. In cellular systems anchors are identified with the base stations. Often, but not always, anchors share a synchronized clock. A certain degree of synchronization is needed to achieve precise positioning. In recent years there has been a rising interest in cooperative positioning systems, where agents can act as anchors for other nodes when their position is known within a certain degree of accuracy [14, 15, 30].

1.3.2 Overview of the positioning process

Regardless of the network structure, the task of positioning in a wireless network consists of two steps: the measurement phase and the location update phase.

In the measurement phase, nodes measure the physical properties of interest from the wireless signal, to infer information on the relative position of nodes. See Section 1.3.3 for more details.

In the location update phase, each agent determines its own position based on the information acquired during the measurement phase and any previously available information, such as the last agent position and the location of anchors. The update process can be computed locally by agents (distributed positioning) or by anchors and then transmitted to agents over the network (centralized positioning).

These steps are performed sequentially every time the position information needs to be updated. The present thesis works focuses on the measurement phase, in particular on the estimation of the ToA.

1.3.3 Classification of positioning systems

Existing positioning methods can be classified in several ways. Different subdivisions can be defined depending on the parameter of choice, such as topology, territorial coverage, and the physical quantity that is measured to obtain the positioning information [31]. An overview of the possible classification criteria follows, including some examples.

When the provided physical coverage is considered, positioning systems can be classified as satellite, terrestrial, or short-range.

- Satellite localization methods rely on a constellation of satellites to provide positioning services on a global scale. An obvious example is

the GPS.

- Terrestrial systems are based on signals broadcast by land-bound stations. Terrestrial systems may be dedicated, such as the LOng RAnge Navigation (LORAN) system, or integrated in a multi-purpose network like in the LTE standard. Terrestrial systems need base stations to be deployed in the whole area to be covered, depending on the employed communication technology.

- Short-range localization systems provide positioning in small areas such as a single building or building complex, and are well suited for indoor positioning [32]. Often, short-range positioning systems are based on WLAN technologies, sensor networks, or on dedicated anchors [4, 5].

Positioning systems can also be subdivided in integrated, opportunistic or hybrid systems based on their intended purpose.

- Integrated systems are developed specifically for positioning purposes. Examples include the GNSS systems and the LORAN.

- Opportunistic systems exploit protocols developed for different purposes than localization. Such systems are of particular interest because they allow positioning information to be inferred without the need to allocate dedicated transmission resources and hardware and without changing the existing technology and protocols. However, Signals of Opportunity (SoP) are generally more difficult to exploit than dedicated ones.

- Hybrid systems employ a mixture of dedicated and opportunistic approach in an adaptive fashion. The LTE network can act as a hybrid

system when both the positioning protocol and signals of opportunity are exploited.

Positioning systems are usually classified taking in consideration the physical quantities that are exploited to determine the relative position of nodes. In this case, systems can be subdivided as follows.

Time of Arrival (ToA) In ToA-based ranging systems, the distance between nodes is estimated by measuring the time a signal takes to propagate between the transmitter and the receiver. ToA-based positioning techniques are explained in greater detail in Section 1.4.

Time Difference of Arrival (TDoA) The TDoA method has the advantage of not needing tight synchronization between the agents, but only for anchor nodes. This is easier to exploit since anchors are usually fixed. The anchors transmit a reference signal at the same time, and the mobile terminal estimates the ToA relative to each anchor. Then for each possible pair of anchors the difference between the ToA is evaluated, leading to an estimation of the differential distance between the two anchors and the receiver. Being $\hat{\tau}^{(1)}$ and $\hat{\tau}^{(2)}$ the ToA estimations from a pair of anchors, the differential distance is estimated as:

$$\hat{\Delta}d = c(\hat{\tau}^{(2)} - \hat{\tau}^{(1)}) \tag{1.13}$$

This is not an actual distance measurement, but it can be exploited for localization techniques such as hyperbolic positioning [25].

Received Signal Strength (RSS) The RSS-based method exploits the dependence on the distance of the received signal power. The mobile node measures the received power level and determines the distance from the anchor. The propagation model needs to be determined beforehand and

affects the accuracy of the estimation greatly. A simple propagation model that is often used in general cases is the following:

$$P_{r,dB} = P_{t,dB} - 10\alpha \log_{10}(d) - K - X_f - X_s \tag{1.14}$$

where $P_{r,dB}$ and $P_{t,dB}$ are the received and transmitted powers expressed in dB, K is a constant factor depending on the antenna gains, X_f is a random variable that models fading, X_s models shadowing, and the logarithmic term models the attenuation due to distance depending on the path loss exponent α. Assuming knowledge of all the parameters, the distance d can easily be estimated by inverting (1.14) after the path loss exponent α has been estimated:

$$\hat{d} = 10^{-\frac{P_{r,dB} - P_{t,dB} + K}{10\alpha}} \tag{1.15}$$

The fading and shadowing terms can be removed if enough samples are accumulated, due to the fast variation rate. More complex propagation models have been developed for specific scenarios and can be found in [33]. Usually, a receiver module already has the received signal power information, thus most RSS-based systems are fully opportunistic. The downsides of RSS-based method include the requirement of extensive mapping campaigns before the system can be deployed and the sensitivity to environment changes. An example of such techniques can be found in [34].

Differential Received Signal Strength (DRSS) Similarly to TDoA, the DRSS method estimates the differential distance between the nodes to be positioned and the anchor. It exploits the difference between the powers received from a pair of anchors, using (1.15) to estimate the differential distance between agents.

Direction of Arrival (DoA) In DoA measurements, an array of receiving antennas is exploited to determine the angle of incidence of the incoming signal, with respect to a fixed direction. However, the need of multiple antennas at the receiver limits its usefulness for small-sized mobile terminals. DoA techniques are usually employed in radar systems.

Power Delay Profile (PDP) These methods are based on the shape of the estimated Power Delay Profile of the channel. This can be used to obtain ToA or TDoA estimations by selecting the first peak in the PDP that exceeds a given threshold or the one with the greatest amplitude. More refined methods have been developed to overcome the inherent sensibility to multi-path propagation of PDP based methods.

Node ID In node ID based positioning methods, each anchors transmit its own unique ID as part of the reference signal. ID-based positioning is very simple to implement, but it generally has poor performance and needs densely deployed anchors to operate. For example, in a cellular network the Base Station identifier can be used to locate the mobile terminal, based on the coverage area of the Base Station the terminal is currently associated to. Node ID based positioning techniques are also referred to as proximity-based.

Others Some positioning methods do not fall into any of the above categories. One example is presented in [35], where the author propose a model-order based criteria to discriminate the reference signals,

A novel category of positioning methods is that of cooperative localization [36]. Cooperative localization might employ any of the mentioned ranging

methods to obtain an estimation of the distance between nodes. When cooperative localization is performed, the roles of agents and anchors are not completely separated: any node can act as anchor provided its own position is known with a certain degree of accuracy. In [15], cooperative positioning is achieved using the message-passing algorithm [37]. It however becomes necessary to estimate the distances between mobile agents as well as the distance between agents and anchors, adding a substantial number of unknowns and measurements. The positioning information also needs to be exchanged between nodes, requiring additional resources for transmission and computation.

1.4 Time of Arrival-based Positioning

In ToA-based radio positioning systems the distance between two nodes is estimated by measuring the time of travel of the electromagnetic signal between the transmitter and the receiver. In radio propagation it can be assumed that the signal travels at the speed of light c, which is approximately equal to $3 \times 10^8 m/s$.

ToA based ranging is trivial to perform under the assumption that the clocks of all the nodes are perfectly synchronized. The transmitter (anchor) can include the timestamp of transmission time T_t in the reference signal. The receiver simply measures the time of reception of the reference signal T_r and the distance between the nodes can be determined as:

$$\hat{d} = (T_r - T_t)c \tag{1.16}$$

An example of ToA estimation in a synchronized environment is proposed in Fig. 1.8. However, such a degree of synchronization is difficult to achieve and often beyond that needed for communication purposes. In satellite-based

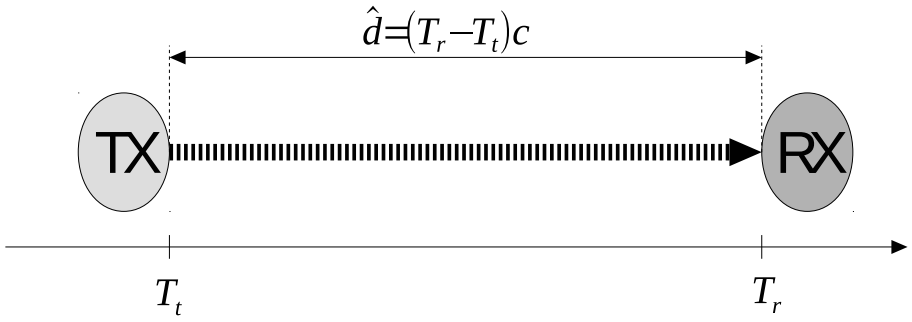

Figure 1.8: ToA estimation with synchronized nodes.

systems, atomic clocks are employed to tightly synchronize the transmitters. In most practical cases nodes lack such synchronization.

Now assume that the receiver clock has an offset e_s compared to the transmitter clock, as shown in Fig. 1.9. The receiver measures the time of arrival T_r according to its own clock, however the timestamped time of transmission T_t is measured with respect to the transmitter's clock. In this case, the estimated range does not depend only on the distance but also on the error. As such the calculated range is referred to as pseudo-range and it is equal to $\hat{p} = (T_r - T_t)c$. To compensate this error the clock offset e_s needs to be estimated in some way. The actual range can then be obtained by correcting the pseudo-range as:

$$\hat{d} = (T_r - T_t)c - e_s c = \hat{p} - e_s c \tag{1.17}$$

An example of this behavior is proposed in Fig. 1.9.

There are many methods to estimate the clock offset e_s. The GPS for instance implements its own technique to compensate for the receiver clock offset [27], while other techniques have been developed for terrestrial systems that require a certain number of anchors to estimate the offset.

Distance estimation based on ToA measurements presents other issues

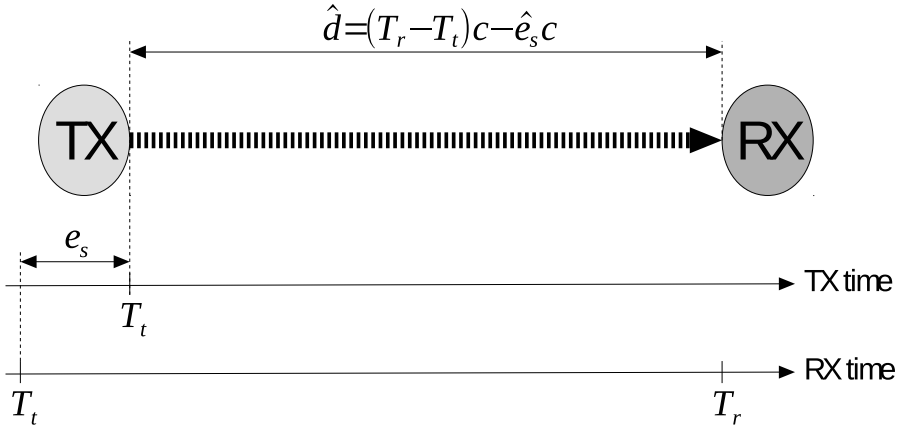

Figure 1.9: ToA estimation with non-synchronized nodes.

that need to be addressed to obtain a reliable, usable estimate. The most important issue is related to the propagation environment, which is often characterized by multi-path propagation.

Satellite-based positioning systems rarely exhibit multi-path propagation, except in condition of limited sky visibility where the positioning service is often disrupted. In land-based systems however multi-path is almost always present. The propagation time between the station and the mobile terminal is only related to ToA if the signal propagates through Line of Sight (LoS). The presence of secondary, non-Line of Sight (NLoS) paths may severely impair the estimation of the LoS ToA. Indeed, several signal processing techniques have been devised to separate the direct path from the indirect paths. In case of shadowing the LoS path may not be present at all, causing an inherent bias in the distance estimation even when the shortest path is correctly recognized.

The accuracy achievable by ToA estimation techniques depends directly on the available bandwidth of the reference signal [38] and on the nature of the propagation environment [39]. When high positioning precision is

required, a wide transmission band needs to be employed. Under this perspective, LTE becomes an interesting standard for positioning because of its reasonably high bandwidth and band-spanning reference signals described in Sections 1.2.3 and 1.2.4.

1.5 Trilateration

Estimating the distance $\hat{d}$ between the agent and the anchor accounts for the measurement phase of ToA-based positioning. Most often in ToA-based positioning, the location update phase is performed by means of the trilateration technique. Trilateration consists of finding the intersection of a set of circles centered in the anchors' positions, with a radius equal to the respective measured ranges.

For simplicity's sake, the 2-dimensional (2-D) trilateration is considered, although the problem can be extended to the 3-D case easily. Let $\boldsymbol{p}_i \in \mathbb{R}^2$, $i = 1, \ldots, M$ be the (known) positions of the anchors and $\hat{d}_i$, $i = 1, \ldots, M$ the respective estimated distances of the agent from the anchors. The position of the agent $\boldsymbol{p}$ can be determined by solving the trilateration problem, which corresponds to:

$$\begin{cases} ||\boldsymbol{p} - \boldsymbol{p}_1|| &= \hat{d}_1 \\ ||\boldsymbol{p} - \boldsymbol{p}_2|| &= \hat{d}_2 \\ \ldots & \\ ||\boldsymbol{p} - \boldsymbol{p}_M|| &= \hat{d}_M \end{cases} \tag{1.18}$$

This is a non-linear system of equations. In the 2-D positioning case, at least 3 visible anchors are needed to update the location of the agent without ambiguities (hence the name trilateration). However, real life range estimation may be affected by errors. Hence, to obtain a position estimation from (1.18), approximate methods such as least-square estimation are required.

Another problem affecting trilateration is the lack of synchronization between the nodes. Assuming synchronization between each anchor (this is true in GNSS systems, where satellites are equipped with high-precision atomic clocks), only the time offset of the agent e_s needs to be estimated. The offset is treated as an additional unknown variable to determine in the equation system. The pseudo-ranges between the agent and each anchor are defined:

$$\hat{\rho}_i = d_i + e_s c \tag{1.19}$$

leading to the following set of equations:

$$\begin{cases} ||\boldsymbol{p} - \boldsymbol{p}_1|| + e_s c & = \hat{\rho}_1 \\ ||\boldsymbol{p} - \boldsymbol{p}_2|| + e_s c & = \hat{\rho}_2 \\ \dots & \\ ||\boldsymbol{p} - \boldsymbol{p}_M|| + e_s c & = \hat{\rho}_M \end{cases} \tag{1.20}$$

Because an additional variable is present, the minimum number of equations (and thus of visible anchors) required increases by one as well.

2 OFDM-based ToA Estimation Algorithms

In this chapter the novel algorithms developed for the estimation of ToA in OFDM systems are presented. Two methods are proposed: the Slope-based algorithm and the Difference-Based algorithm. Both exploit the physical properties of OFDM transmission to obtain a ToA estimation. These methods can be applied to any communication system using OFDM, and are easily scalable.

The Slope-Based algorithm is meant as a low-complexity method to obtain a quick delay estimation when the propagation conditions are favorable, that is, there is a strong Line of Sight (LOS) propagation. It is applied on a symbol basis, processing one OFDM symbol at a time.

The Difference-Based algorithm, on the other hand, can be applied to multiple consecutive symbols at once and it can provide an accurate estimation of the first propagation path delay even when strong secondary paths are present. It does however require a large computational complexity when compared to the simple Slope-Based algorithm.

2.1 The Slope-Based ToA Estimation Algorithm

In a multi-path propagation environment, each of the L paths is characterized by its complex amplitude coefficient $\alpha_l = |\alpha_l|e^{j\phi_l}$ and by its delay τ_l. The delays are assumed to be different from each other and ordered increasingly (that is, $\tau_1 < \tau_2 < \ldots < \tau_L$) for the sake of simplicity. The weights are assumed to be independent from each other. The expression of the Channel Impulse Response referred to a single-band channel is reported here for convenience.

$$h(t) = \sum_{l=1}^{L} \alpha_l \delta(t - \tau_l) \tag{2.1}$$

Consider now the Channel Frequency Response, given by the Fourier transform of (2.1):

$$H(f) = \sum_{l=1}^{L} \alpha_l e^{-j2\pi f \tau_l} \tag{2.2}$$

In the baseband representation of an OFDM system, the sub-carrier frequencies are given by $f = k\Delta f$, $k \in \mathcal{K}$. Now consider a noiseless channel with a single propagation path ($L = 1$). The CFR becomes:

$$H_1(f) = \alpha_1 e^{-j2\pi k \Delta f \tau_1}, \quad k \in \mathcal{K} \tag{2.3}$$

In this case, the phase rotation induced by the propagation channel for each sub-carrier is given by:

$$\rho(\tau_1, k) = \arg\left\{\alpha_1 e^{-j2\pi k \Delta f \tau_1}\right\} = \arg\{\alpha_1\} - 2\pi k \Delta f \tau_1 \tag{2.4}$$

which decreases linearly with the sub-carrier index k. The phase difference between two adjacent sub-carriers results:

$$\begin{aligned} \rho(\tau_1, k+1) - \rho(\tau_1, k) &= \arg\{\alpha_1\} - 2\pi\tau_1(k+1)\Delta f \\ &\quad - (\arg\{\alpha_1\} - 2\pi\tau_1 k \Delta f) = -2\pi\tau_1\Delta f \end{aligned} \tag{2.5}$$

The difference does not depend on the argument of α_1. This property can be exploited to obtain a delay estimation by inverting (2.5). The ranging method of [40] employs the phase difference between two sole sub-carriers in this fashion. Now consider the phase rotation for a two-path channel ($L = 2$), which is given by:

$$\begin{aligned}\rho(\tau, k) &= \arg\left\{\alpha_1 e^{-j2\pi k\Delta f\tau_1} + \alpha_2 e^{-j2\pi k\Delta f\tau_2}\right\} = \\ &= \arg\left\{\alpha_1 e^{-j2\pi k\Delta f\tau_1}\left(1 + \frac{\alpha_2}{\alpha_1} e^{-j2\pi k\Delta f(\tau_2-\tau_1)}\right)\right\}\end{aligned} \tag{2.6}$$

It can be shown that if $|\alpha_1|/|\alpha_2| > 1$, the slope trend of the unwrapped phase across the sub-carrier frequencies holds significant information on the first path delay τ_1. Thus, phase unwrapping and least-squares linear fitting can be used to obtain a delay estimation if a large enough interval of frequencies is available. If $|\alpha_2|/|\alpha_1| > 1$, the unwrapping and fitting procedure can be used to obtain τ_2 instead. In the general case with $L > 2$ paths, τ_i can be easily determined by means of linear fitting if the i-th propagation channel satisfies the following dominance condition:

$$|\alpha_i| > \sum_{\substack{l=1 \\ l\neq i}}^{L} |\alpha_l| \tag{2.7}$$

If the phase rotation between adjacent sub-carriers is greater than 2π, a wraparound occurs that causes an estimation bias. As such, the wraparound condition is defined:

$$\rho(\tau_1, k+1) - \rho(\tau_1, k) < 2\pi \tag{2.8}$$

This limits the range of τ_1 values that can be correctly estimated without bias. After some manipulation:

$$\tau_1 \Delta f \ll 1 \tag{2.9}$$

Under these sufficient conditions, the linear fitting of the unwrapped phase will hold significant information on the delay of the dominant channel. Some examples are included in [41], where the effects of the unwrap procedure on the linear estimation of the slope are assessed. To this end, a full baseband OFDM system has been simulated in multi-path and noisy conditions.

2.1.1 The unwrap algorithm

The Slope-Based method employs a standard algorithm to unwrap the channel phase samples. The following pseudocode, which illustrates the unwrap procedure, is reported for convenience. More advanced unwrap algorithms have been developed, some with the purpose of being used for delay estimation [42, 43, 44].

Algorithm 1 Listing of the Phase Unwrap procedure.

```
1: procedure VectorUnwrap
2:     output(0) ← input(0)
3:     for i from 1 to length(input) do
4:         diff ← UNWRAP(input(i), input(i − 1))
5:         output(i) ← output(i − 1) + diff
       return output
6: procedure Unwrap
7:     d ← new_angle − previous_angle
8:     if d > π then
9:         diff ← d − 2π
10:    else
11:        if d < −π then
12:            diff ← d + 2π
13:        else
14:            do nothing
       return diff
```

2.1.2 Slope Estimation Algorithm and Piecewise Variant

The available information at the receiver is $\hat{H}[k]$, $k \in \mathcal{K}$, which is a sampled and noisy version of the channel frequency response over a single OFDM symbol. The estimated CFR is calculated as per (1.12). The channel phase is then evaluated as:

$$\hat{\phi}(k) = \arg\left\{\hat{H}[k]\right\} \tag{2.10}$$

The phase is then unwrapped using the standard algorithm of 2.1.1 to obtain $\hat{\phi}_{\mathrm{uw}}[k]$. The phase slope is estimated by applying the least squares linear fitting algorithm to the unwrapped phase vector.

This procedure will yield two coefficients β_0 and β_1, representing the vertical offset and the slope of the best linear approximation. The estimation of the ToA $\hat{\tau}_1$ can easily be obtained as:

$$\hat{\tau}_i = -\frac{\beta_1}{2\pi} \tag{2.11}$$

assuming that the first propagation path satisfies the dominance condition (2.7) and the wraparound condition (2.9). However, the correct estimation of τ_1 is still impaired by the presence of secondary propagation paths even when the dominance condition is verified. The presence of noise also affects the estimation, in particular the unwrap procedure, where it can cause spurious 2π phase jumps. Hence, a piecewise variant of the slope estimation technique is introduced to compensate the effect of noise at low SNR.

To perform piecewise linear fitting, the set of observed sub-carrier frequencies $\mathcal{K}$ is subdivided in a number U of contiguous sub-sets k_u, each containing N_{k} elements so that:

$$\mathcal{K} = \bigcup k_u \quad u = 1, \ldots, U \tag{2.12}$$

The length of the sub-interval is chosen so that N is a multiple of N_{k}. Similarly, the set of unwrapped channel phase rotations $\hat{\phi}_{\mathrm{uw}}[k]$ is subdivided in

U sub-sets $\hat{\phi}_u[k]$, so that:

$$\hat{\phi}_{\mathrm{uw}}[k] = \bigcup \hat{\phi}_u \quad u = 1, \ldots, U \tag{2.13}$$

This way, $\hat{\phi}_u$ contains the phase values corresponding to the set of sub-carrier frequencies k_u. Each k_u,$\hat{\phi}_u$ pair can be considered as an OFDM system on its own, with a number of sub-carriers equal to N_{k}.

Then, the linear fitting procedure is applied to each k_u,$\hat{\phi}_u$ pair, obtaining U slope estimations $\beta_{1,u}$. The sample mean μ_β and standard deviation σ_β of the estimations set are calculated as:

$$\mu_\beta = \frac{1}{U} \sum_{q=u}^{U} \beta_{1,u} \tag{2.14}$$

$$\sigma_\beta = \sqrt{\frac{1}{U-1} \sum_{u=1}^{U} (\beta_{1,u} - \mu_\beta)^2} \tag{2.15}$$

At this point, outliers need to be removed from the set of estimated slopes. All the values $\beta_{1,u}$ that do not satisfy the condition:

$$|\beta_{1,u} - \mu_\beta| \leq r\sigma_\beta \tag{2.16}$$

where r is a suitable coefficient, are discarded. Let $\mathbb{U}$ be the set of indexes u so that the $\beta_{1,u}$ satisfy the condition of Eq. (2.16). A new mean is calculated using the $U' < U$ remaining values, where U' is the cardinality of $\mathbb{U}$.

$$\mu'_\beta = \frac{1}{U'} \sum_{u \in \mathbb{U}} \beta_{1,u} \tag{2.17}$$

The estimated delay is finally calculated as:

$$\hat{\tau}_i = -\frac{\mu'_\beta}{2\pi} \tag{2.18}$$

The outliers removal procedure is of crucial importance for the piecewise Slope-Based delay estimation. It has been shown [45] that without outliers

N	1024
N_{cp}	128
Δf [kHz]	15
r	3

Table 2.1: Simulation Parameters for the Slope-Based Algorithm.

removal, the piecewise method does not yield any advantage at lower SNR values, while presenting worse performance at high SNR compared to regular linear fitting.

2.1.3 Slope-Based Estimation Results

An accurate simulator is implemented to assess the performance of linear fitting slope estimation and its piecewise variant with outliers removal in multi-path channels. The simulation software is written in the C++ language, with the inclusion of the ALGLIB libraries [46] which provided an efficient implementation of the linear fitting procedure.

The COST207 4-taps and 6-taps channel models for rural areas [47] were chosen for the simulations. The simulation parameters are reported in Table 2.1. It is assumed that the phase rotation information is available for all the sub-carriers. The results for the COST207 4-taps channel are shown in Fig. 2.1. It can be seen that piecewise linear fitting slope estimation generally outperforms regular linear fitting, with the smallest values of N_{k} having the best performance at low SNR and the largest values working better at high SNR.

For the 6-taps channel, the simulated results are reported in Fig. 2.2. Because of the larger number of secondary paths, the dominance condition

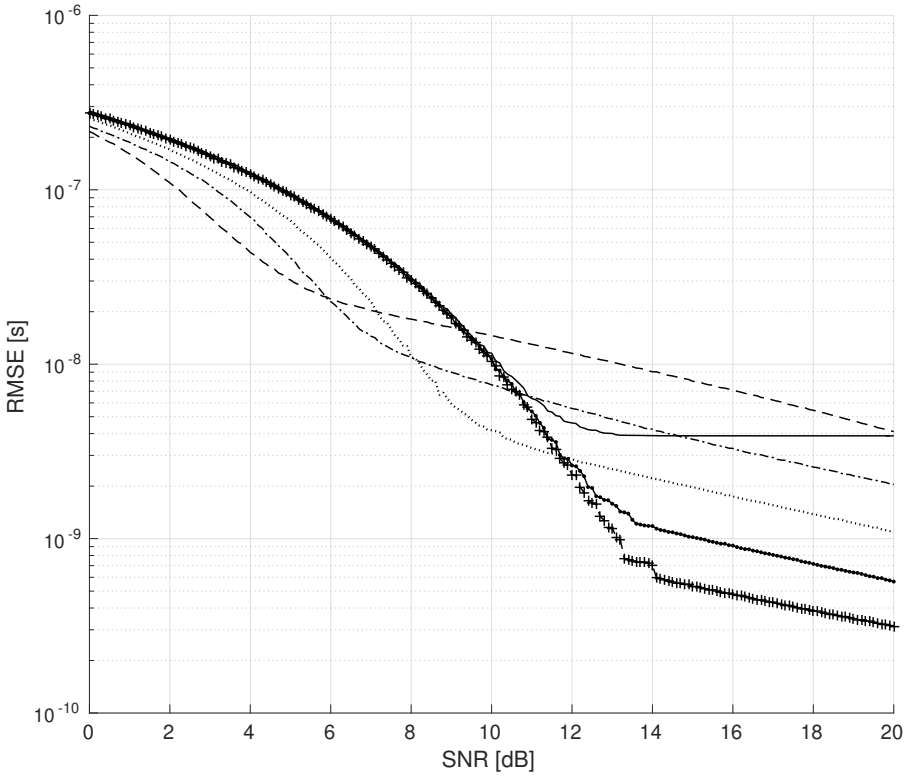

Figure 2.1: RMSE performance for Slope-Based and piecewise Slope-Based estimation on the COST 207 RA4 channel. –: Regular Linear Fitting. ——: $N_{\mathrm{k}} = 16$. —·: $N_{\mathrm{k}} = 32$. ·· : $N_{\mathrm{k}} = 64$. •: $N_{\mathrm{k}} = 128$. +: $N_{\mathrm{k}} = 256$.

of (2.7) is less likely to be satisfied with respect the 4-taps channel, leading to a different behavior. The value $N_{\mathrm{k}} = 256$ has the overall best performance, with smaller values of N_{k} presenting better performance at low SNR. It can be seen that at low SNR, a denser subdivision of the available carriers outperforms regular linear fitting. The larger number U of estimates compensates for the loss in Gabor bandwidth at lower values of the interval length. For higher SNRs, a larger value of N_{k} is optimal, and when the SNR is very high the best performance is given by regular linear fitting over the

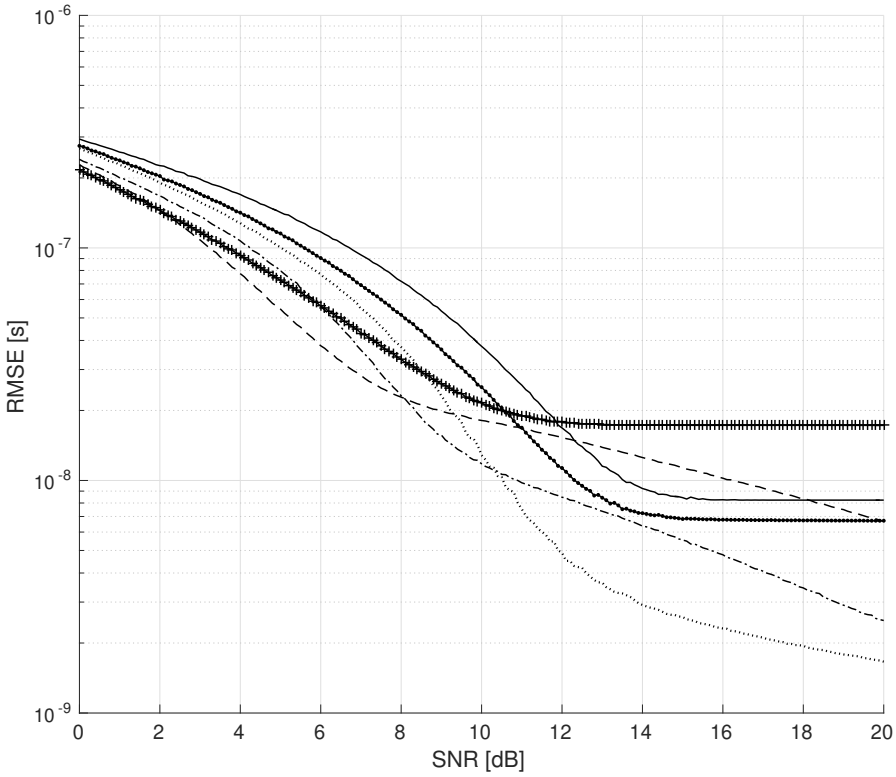

Figure 2.2: RMSE performance for Slope-Based and piecewise Slope-Based estimation on the COST 207 RA6 channel. –: Regular Linear Fitting. −−: $N_{\mathrm{k}} = 16$. −·: $N_{\mathrm{k}} = 32$. ·· : $N_{\mathrm{k}} = 64$. •: $N_{\mathrm{k}} = 128$. +: $N_{\mathrm{k}} = 256$.

whole bandwidth. This suggests the use of an adaptive estimation algorithm, that employs different values of N_{k} according to the estimated SNR if such information is available. In all cases, the value $r = 3$ has been chosen for the outliers removal procedure.

2.2 The Difference-Based ToA Estimation Algorithm

In the absence of noise (2.2) can be rearranged as:

$$\begin{aligned} H(f) &= \sum_{l=1}^{L} A_l e^{j(\phi_l - 2\pi f \tau_l)} \\ &= A_1 e^{j(\phi_1 - 2\pi f \tau_1)} \left\{ 1 + \sum_{l=2}^{L} \frac{A_l}{A_1} e^{j[\phi_l - \phi_1 - 2\pi f(\tau_l - \tau_1)]} \right\} \end{aligned} \tag{2.19}$$

where $\alpha_l = A_l e^{j\phi_l}$. The argument of $H(f)$ may be written, after some manipulations, as:

$$\begin{aligned} \Phi(f) &= \arg\{H(f)\} \\ &= \phi_1 - 2\pi f \tau_1 + \arctan\left[\frac{Y_1(f)}{X_1(f)}\right] \end{aligned} \tag{2.20}$$

where $X_1(f)$ and $Y_1(f)$ are defined as:

$$X_1(f) = \sum_{l=1}^{L} B_l \cos(\Delta\phi_l - 2\pi f \Delta\tau_l) \tag{2.21a}$$

$$Y_1(f) = \sum_{l=1}^{L} B_l \sin(\Delta\phi_l - 2\pi f \Delta\tau_l) \tag{2.21b}$$

The following substitutions were made:

$$B_l = \frac{A_l}{A_1} \tag{2.22a}$$

$$\Delta\phi_l = \phi_l - \phi_1 \tag{2.22b}$$

$$\Delta\tau_l = \tau_l - \tau_1 \tag{2.22c}$$

Now, take in account the first frequency derivative of (2.20), which is given by:

$$\Phi'(f) = -2\pi \left[\tau_1 + \frac{X_1(f)X_2(f) + Y_1(f)Y_2(f)}{X_1^2(f) + X_2^2(f)}\right] \tag{2.23}$$

where the following substitutions were made:

$$X_2(f) = \sum_{l=1}^{L} B_l \Delta\tau_l \cos(\Delta\phi_l - 2\pi f \Delta\tau_l) \tag{2.24a}$$

$$Y_2(f) = \sum_{l=1}^{L} B_l \Delta\tau_l \sin(\Delta\phi_l - 2\pi f \Delta\tau_l) \tag{2.24b}$$

The purpose of this formulation is to obtain an estimate of the propagation delay τ_1 corresponding to the shortest path. To this aim, inverting (2.23) with respect to τ_1, one obtains:

$$\tau_1 = -\frac{\Phi'(f)}{2\pi} - \frac{X_1(f)X_2(f) + Y_1(f)Y_2(f)}{X_1^2(f) + X_2^2(f)} \tag{2.25}$$

A good estimate for $\Phi'(f)$ can be derived from the difference quotient of the measured channel phase. This phase estimation may be performed recalling (1.11), from which one can define:

$$\hat{H}[k] = \frac{Y[k]}{\tilde{X}[k]} = NH[k] + \hat{n}[k], \qquad k = 0, \ldots, N-1 \tag{2.26}$$

where $\hat{n}[k] = \tilde{n}[k]/\tilde{X}[k]$. From (1.12), in fact, the required difference quotient may be evaluated as:

$$\hat{\Phi}'(k) = \frac{\hat{\phi}(k+1) - \hat{\phi}(k)}{\Delta f}, \quad k \in \mathcal{K}' \tag{2.27}$$

where $\mathcal{K}' = \mathcal{K} - \{N/2\}$ is the set of all sub-carriers except the last one and the estimated phase $\hat{\phi}(k)$ is given by:

$$\hat{\phi}(k) = \arg\left\{\hat{H}[k]\right\}, \quad k \in \mathcal{K} \tag{2.28}$$

These values are substituted into (2.25) to obtain a generic estimation of τ_1 as a function of $\hat{\Phi}'(k)$:

$$\hat{\tau}_1\left[\hat{\Phi}'(k)\right] = -\frac{X_1(k\Delta f)X_2(k\Delta f) + Y_1(k\Delta f)Y_2(k\Delta f)}{X_1^2(k\Delta f) + X_2^2(k\Delta f)} - \frac{\hat{\Phi}'(k)}{2\pi} \tag{2.29}$$

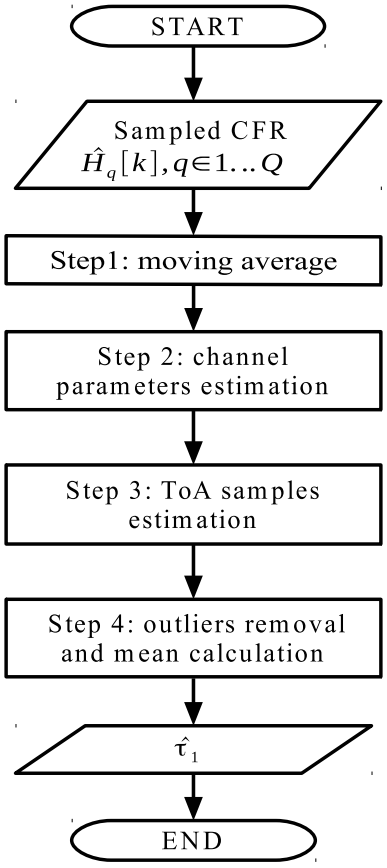

Figure 2.3: Flowchart of the DBTE algorithm.

To improve the accuracy of (2.29), which may suffer from noise effects, a Difference-Based approach is proposed in this section. The resulting DBTE algorithm is organized in four steps (Fig. 2.3), which are described in detail in the following paragraphs.

2.2.1 The DBTE Algorithm step-by-step

Step 1: moving average The algorithm receives as input a sequence of sampled CFRs $\hat{H}_1[k], \ldots, \hat{H}_q[k], \ldots, \hat{H}_Q[k]$, measured over several Q consecutive symbols. Let $N_s (\leq N)$ be the number of OFDM sub-carriers carrying reference symbols that are actually employed for the

CFR calculation. As a first step, to smooth the noise effect over time-consecutive symbols, a moving average with window length equal to $l_w = 2l_h + 1$, with $l_h \in \mathbb{N}$, $l_h \geq 1$, $l_w < Q$ is applied in the time direction. This results into a filtered version of the sampled CFR, which provides $Q - 2l_h$ samples for each sub-carrier. Thus, for the k-th sub-carrier ($k \in \mathcal{K}$), the p-th sample may be expressed as:

$$\bar{H}_p[k] = \frac{1}{l_w} \sum_{u=p}^{p+2l_h} \hat{H}_u[k], \qquad p \in \mathcal{P} \tag{2.30}$$

where $\mathcal{P} = \{1, \ldots, Q-2l_h\}$ is the set of the symbol indexes. These samples are grouped in the $N_s \times (Q-2l_h)$ matrix $\mathbf{H} = \left[\bar{H}_1[k] \ldots \bar{H}_{Q-2l_h}[k]\right]$.

Step 2: channel parameter estimation The second step involves the estimation $\hat{L}$ of the number of paths L, which is subsequently used to estimate the $\hat{L}$ normalized amplitudes B_l, the $\hat{L}$ relative phases $\Delta\phi_l$, and the $\hat{L} - 1$ differential delays $\Delta\tau_l$ required by (2.21) and (2.24). The easiest way to obtain these estimates is to calculate the Channel Impulse Response (CIR) $\hat{h}[n]$ by performing an IDFT operation. The first symbol (column) of $\mathbf{H}$ is chosen for this purpose by assuming that the CIR does not vary significantly over Q consecutive symbols. The absolute value of the CIR results into a N-sequence $|\hat{h}[n]|$. A minimum threshold ξ is used to detect the $\hat{L}$ peaks corresponding to the ToAs of the different paths displayed by the CIR. The index values $\bar{n}_1, \ldots, \bar{n}_{\hat{l}}, \ldots, \bar{n}_{\hat{L}}$ for which $|\hat{h}[\bar{n}_{\hat{l}}]| > \xi$ holds true are stored. Therefore, B_l, $\Delta\phi_l$ and $\Delta\tau_l$ in (2.22) are estimated, respectively, as:

$$\hat{B}_{\hat{l}} = \frac{|\hat{h}[\bar{n}_{\hat{l}}]|}{|\hat{h}[\bar{n}_1]|}, \qquad \hat{l} = 1, \ldots, \hat{L} \tag{2.31a}$$

$$\widehat{\Delta\phi}_{\hat{l}} = \arg\{\hat{h}[\bar{n}_{\hat{l}}]\} - \arg\{\hat{h}[\bar{n}_1]\}, \quad \hat{l} = 1, \ldots, \hat{L} \tag{2.31b}$$

$$\widehat{\Delta\tau}_{\hat{l}} = (\bar{n}_{\hat{l}} - \bar{n}_1)T, \qquad \hat{l} = 1, \ldots, \hat{L} \tag{2.31c}$$

from which, by (2.21) and (2.24), one obtains $X_1(f)$, $Y_1(f)$, $X_2(f)$ and $Y_2(f)$.

Step 3: ToA samples estimation As a third step, considering the measured differential phases $\hat{\Phi}'_p(k)$ for $p \in \mathcal{P}$ and $k \in \mathcal{K}'$ provided by (2.27) and (2.28), one can evaluate the set of $U = (N_s - 1)(Q - 2l_h)$ estimates:

$$\hat{\tau}_1^{p,k} = \hat{\tau}_1\left[\hat{\Phi}'_p(k)\right], \qquad p \in \mathcal{P}, k \in \mathcal{K}' \tag{2.32}$$

The elements of the set defined by (2.32) are in general affected by noise and may suffer from a systematic error due to phase wraparounds. Thus, an additional step is needed to refine the final estimation.

Step 4: outliers removal and mean calculation The first operation performed in the fourth step is the outliers removal. To this aim, the mean and the standard deviation of the set defined by (2.32) are calculated as:

$$\mu = \frac{1}{U}\sum_{p\in\mathcal{P}}\sum_{k\in\mathcal{K}'}\hat{\tau}_1^{p,k} \tag{2.33}$$

$$\sigma = \sqrt{\frac{1}{U-1}\sum_{p\in\mathcal{P}}\sum_{k\in\mathcal{K}'}(\hat{\tau}_1^{p,k} - \mu)^2} \tag{2.34}$$

A subset $\mathcal{U}$ of index pairs (p, k) is now defined by selecting the estimates satisfying the relationship $|\hat{\tau}_1^{p,k} - \mu| \leq r\sigma$, where r is a suitable

General		DBTE	
$N = N_s$	1024	Q	100
N_{cp}	128	l_w	25
Δf [kHz]	15	ξ	0.1
Number of simulations	100	r	2
DP [μs]	$[1, 1.2, 1.4, 1.6]$		

Table 2.2: Simulation Parameters for the DBTE Algorithm.

threshold. The second operation carried out at this final step is the evaluation of a novel average calculated over the samples identified by the indexes belonging to $\mathcal{U}$. This finally yields the desired estimation of the ToA for the first path:

$$\hat{\tau}_1 = \frac{1}{U'} \sum_{(p,k)\in\mathcal{U}} \hat{\tau}_1^{p,k} \tag{2.35}$$

where $U' = \mathcal{C}(\mathcal{U})$ is the cardinality of $\mathcal{U}$.

2.2.2 Difference-Based Estimation Results

The developed DBTE algorithm is implemented in MATLAB and its performance is compared with that provided by the Slope-Based algorithm, proposed in 2.1, which exploits the phase rotation of OFDM sub-carriers to obtain a ToA estimation when the first path is also the strongest one. The adopted parameters and settings are reported in Table 2.2.

Figs. 2.4-2.6 show the Root Mean Square Error (RMSE) performance as a function of the Signal-to-Noise Ratio (SNR) for the four compared algorithms in three channel scenarios characterized by different power profiles. In par-

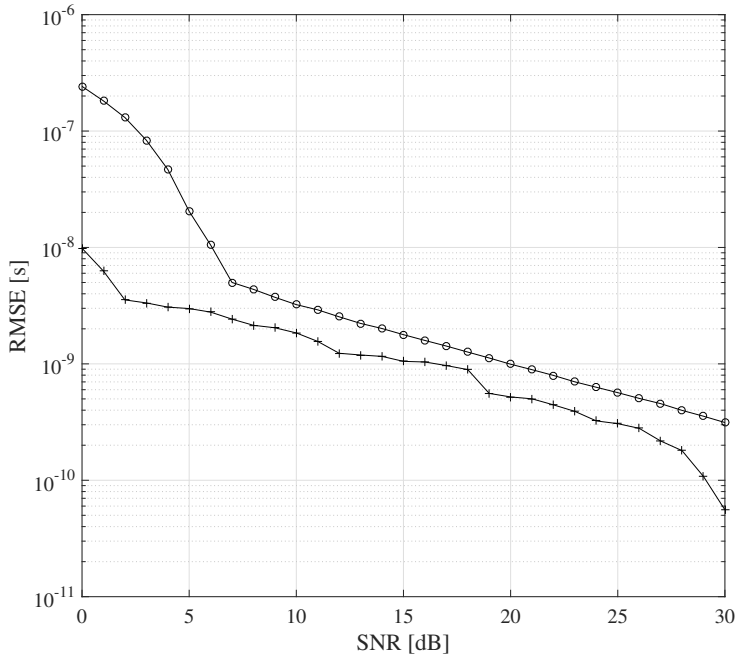

Figure 2.4: ToA estimation for an average power profile [0 -6 -10 -20] dB. ∘: Slope-Based +: DBTE.

ticular, Fig. 2.4 refers to a scenario in which the shortest path is dominant, that is, its average amplitude is higher than the sum of the amplitudes of all the secondary paths. Instead, Fig. 2.5 considers the case of a non-dominant shortest path with the highest average amplitude, while Fig. 2.6 refers to the case of a non-dominant second path with the highest average amplitude. These three situations are selected to check the proposed DBTE algorithm in scenarios where the ToA estimation of the first path becomes more and more difficult. The non-coincidence of the shortest path with the strongest path affects also the Slope-Based algorithm, whose evolution is yet strictly related to the dominance of the shortest path.

The DBTE algorithm outperforms the Slope-Based methods, presenting

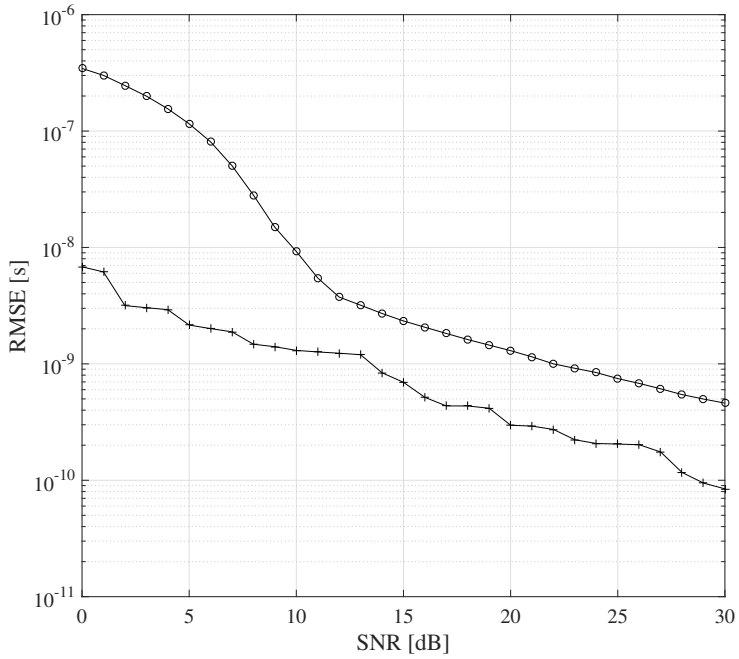

Figure 2.5: ToA estimation for an average power profile = [0 -1 -2 -7] dB. ∘: Slope-Based +: DBTE.

an accuracy that increases with the SNR regardless of the specific scenario. This reveals that the developed solution may be applied in a wide set of situations.

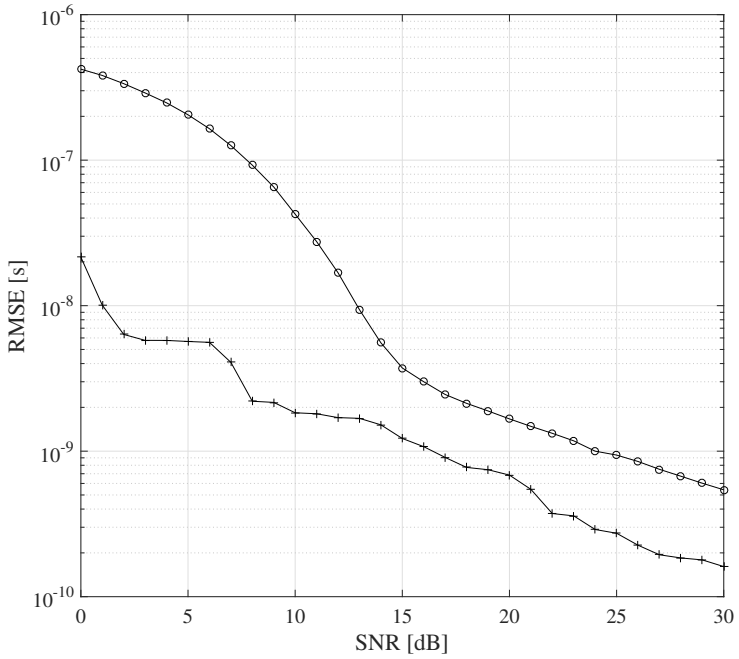

Figure 2.6: ToA estimation for an average power profile [-1 0 -2 -7] dB. ∘: Slope-Based +: DBTE.

3 Multi-Band Time of Arrival Estimation

This chapter presents the work done on the use of multiple frequency bands for the purpose of ToA estimation. The Space Alternating Generalized Expectation-Maximization (SAGE) algorithm was selected, because of its versatility and good performance in complex propagation environments. An overview of SAGE is given starting with its basic principles, then moving to the specific implementations that were used throughout the research work. The advantages of employing multiple transmission bands for the purpose of ToA estimation are assessed through simulations. Two novel methods for combining information inferred from non-synchronized transmission bands, Signal Combining and Signal Aggregating, are then described.

3.1 An overview of the SAGE algorithm

SAGE was first introduced as an extension of the Expectation-Maximization (EM) algorithm [48, 49, 50]. It is a reduced complexity method for the evaluation of the Maximum Likelihood (ML) estimation. More precisely, in SAGE, the multi-dimensional ML estimation problem is subdivided into a certain number of smaller problems to jointly estimate the desired parameters in an iterative way.

An introduction of the EM algorithm is first given, to explain the fundamentals upon which SAGE is based.

3.1.1 The Expectation Maximization Algorithm

Let us consider the adopted L-path channel of (1.8), with $\boldsymbol{\theta}_l = [\mathrm{Re}(\alpha_l), \mathrm{Im}(\alpha_l), \tau_l, \phi_l, f_{D,l}]$ representing the set of parameters of interest for the l-th path. Because L paths are present, the overall set to be estimated is $\boldsymbol{\theta} = [\boldsymbol{\theta}_1, \ldots, \boldsymbol{\theta}_L]$, whose cardinality is equal to $5L$. Let $\mathcal{F}_\mathrm{o}$ be the set of observed sub-carrier frequencies and $\mathcal{T}_\mathrm{o}$ the set of time instants when the CFR is sampled. We define $\bar{H}(f_k, t_s)$, $f_k \in \mathcal{F}_\mathrm{o}$ as the observation of $\hat{H}[k]$ in (1.12) at time t_s. The ML Estimate (MLE) of $\boldsymbol{\theta}$ is then defined as:

$$\hat{\boldsymbol{\theta}}_\mathrm{ML}(\bar{H}) = \arg\max_{\boldsymbol{\theta}}[\Lambda(\boldsymbol{\theta}; \bar{H})] \tag{3.1}$$

being $\hat{\boldsymbol{\theta}}_\mathrm{ML}$ the value of $\boldsymbol{\theta}$ for which the ML function Λ is maximized. The value in (3.1) represents the optimum one, however the maximization operation results computationally prohibitive because of the large dimension of the searching space for large L values. Besides, no general closed formula exists to express the global maximum because of the non-linearity of the function Λ.

The EM algorithm represents a first approach to address the problem.

EM adopts an iterative approach to solve the ML problem in (3.1). It is based upon the distinction between complete data, which are unobservable, and incomplete observable data. With reference to the considered L-paths channel, the CFR can be written as:

$$\begin{aligned} H(f,t;\boldsymbol{\theta}) &= \sum_{l=1}^{L} H_l(f,t;\boldsymbol{\theta}_l) \\ &= \sum_{l=1}^{L} \alpha_l e^{-j2\pi f \tau_l} e^{j2\pi f_{D,l} t} c(\phi_l) \end{aligned} \tag{3.2}$$

where $H_l(f,t;\boldsymbol{\theta}_l)$ for $l = 1,\ldots,L$ is the contribution of the l-th path to the overall CFR. These contributions are assumed independent of each other and their union corresponds to the complete data. No observation $\bar{H}_l(f,t;\boldsymbol{\theta}_l)$ for $l = 1,\ldots,L$ of the complete data is available, hence they must be estimated relying on the incomplete (observable) data $\bar{H}(f,t)$ and on a previous estimation of $\boldsymbol{\theta}$.

The EM algorithm consists of an initialization part and an Expectation (E) and a Maximization (M) step, which are performed at each iteration.

Initialization The initial parameter vector $\boldsymbol{\theta}$ is set to 0. The number L of paths is estimated by means of an appropriate method, such as the Minimum Descriptive Length algorithm [51], resulting into the estimated value $\hat{L}$.

E-step Assuming that the L multipath components are separately observable, it is possible to isolate the contribution of the l-th path from the channel samples to estimate the complete data for the l-th path using the incomplete available data and the current estimation. This is referred to as Parallel Interference Cancellation (PIC): all the impinging waves except for the one to be estimated are cancelled from the channel

observation:

$$\bar{H}_l(f_k,t_s)=\bar{H}(f_k,t_s)-\sum_{l'=1,l'\neq l}^{\hat{L}} H_{l'}(f_k,t_s;\hat{\boldsymbol{\theta}}'_{l'}) \tag{3.3}$$

where $\hat{\boldsymbol{\theta}}'_{l'}$ is a previous estimate of $\boldsymbol{\theta}_l$.

M-step The parameters $\boldsymbol{\theta}_l$ relative to the l-th path (or wave) are estimated as:

$$\hat{\theta}''_l=\hat{\theta}_{l,\mathrm{ML}}=\arg\min_{\boldsymbol{\theta}_l}\left\{\sum_{f_k}\sum_{t_s}||v(f_k,t_s;\boldsymbol{\theta}_l)||^2\right\} \tag{3.4}$$

where:

$$v(f_k,t_s;\boldsymbol{\theta}_l)=\bar{H}(f_k,t_s)-H_l(f_k,t_s;\boldsymbol{\theta}_l) \tag{3.5}$$

for $f_k\in\mathcal{F}_\mathrm{o}$, $t_s\in\mathcal{T}_\mathrm{o}$. With reference to the adopted L-path channel model of (1.8). the delay τ_l, the Angle of Arrival ϕ_l and the Doppler shift $f_{D,l}$ can be estimated first by solving a 3D maximization problem:

$$(\hat{\tau}_l,\hat{\phi}_l,\hat{f}_{D,l})_{ML}=\arg\max_{\tau,\phi,f_D}\left\{\left|z\big(\tau,\phi,f_D;\bar{H}_l(t,f)\big)\right|\right\} \tag{3.6}$$

where z is the 3D correlation function. The complex path amplitude $\hat{\alpha}_l$ is then updated as a function of the estimated parameters $\hat{\tau}_l$,$\hat{\phi}_l$ and $\hat{f}_{D,l}$:

$$\hat{\alpha}_{l,ML}=\frac{z\left(\hat{\tau}_{l,ML},\hat{\phi}_{l,ML},\hat{f}_{D,l})_{ML};\bar{H}_l(f_k,t_s)\right)}{N_\mathrm{R}N_\mathrm{t}||c(\hat{\phi}_{l,ML})||^2} \tag{3.7}$$

where z is the correlation function, N_R is the number of observed channel frequencies and N_t is the number of instants where the CFR was sampled.

Once the full set of parameters of interest $\hat{\boldsymbol{\theta}}_\mathrm{ML}$ is estimated, it is also possible to estimate the noise variance $\hat{\sigma}_n^2$.

3.2 Multi-Band SAGE for ToA Estimation

In a multi-band environment, it is interesting to exploit the information gathered from the overall occupied bandwidth to obtain a more reliable and accurate estimation of the ToA. This is possible if the propagation environment is relatively flat across the whole considered bandwidth. In particular the first propagation path (often, but not always, the direct path) must have similar characteristics across all the considered sub-bands. This is commonly verified and confirmed by observations. An example of a multi-band application of SAGE for ranging purposes is found in [52].

To this purpose, a reduced-complexity implementation of SAGE focused on delay estimation was chosen. The implementation, based on [53], can easily be extended to a multi-band environment, and had been indeed devised to be used in such a scenario. An accurate simulator is implemented in Matlab to infer the possible benefits of dual-band usage and evaluate the ToA estimation performance.

3.2.1 SAGE Implementation

The chosen implementation focuses on the estimation of the ToA. The set of parameters to be estimated is $\boldsymbol{\theta}_l = [\alpha_l, \tau_l]$. To simplify the treatise, it is assumed that the number L of paths is exactly known a-priori. The initialization and the E- and M-steps of the SAGE algorithm, specifically referred to delay and amplitude estimation, can be detailed as follows.

Initialization At iteration $i = 0$ the values to be estimated are initialized to zero, thus:

$$\left[\hat{\tau}_l^{(0)}, \hat{\alpha}_l^{(0)}\right] = [0, 0], \quad l = 1, \ldots, L \tag{3.8}$$

where $\hat{\alpha}_l^{(i)}$ and $\hat{\tau}_l^{(i)}$ denote the estimates of α_l and τ_l at the i-th iteration,

respectively.

E-step The complete data for the l-th path are estimated using the incomplete available data and the current estimation $\left[\hat{\tau}_l^{(i)}, \hat{\alpha}_l^{(i)}\right]$ as:

$$\hat{H}_l^{(i)}(q) = \hat{H}(q) - \sum_{\substack{l'=1 \\ l' \neq l}}^{L} \hat{\alpha}_{l'}^{(i)} \exp\left[-j2\pi f_q \hat{\tau}_{l'}^{(i)}\right] \tag{3.9}$$

for $q = 1, \ldots, N$, where N is the number of observed sub-carrier frequencies.

M-step The delay and amplitude estimates of the l-th path are updated using (3.9) by:

$$\hat{\tau}_l^{(i+1)} = \arg\max_{\tau} \left|\zeta_l^{(i)}(\tau)\right| \tag{3.10}$$

$$\hat{\alpha}_l^{(i+1)} = \frac{\zeta_l^{(i)}\left[\hat{\tau}_l^{(i+1)}\right]}{N} \tag{3.11}$$

where:

$$\zeta_l^{(i)}(\tau) = \sum_{q=1}^{N} \hat{H}_l^{(i)}(q) \exp\left(j2\pi f_q \tau\right) \tag{3.12}$$

identifies the cost function.

3.2.2 Multi-band Simulation Results

This section presents the results obtained from the Matlab implementation of the described SAGE algorithm in a dual-band communication context with contiguous frequency bands. The adopted parameters are reported in Table 3.1, where N_{u_m} $(m = 1, 2)$ is the number of sub-carriers occupied by modulated symbols and N_{s_m} $(m = 1, 2)$ is the number of sub-carriers reserved for the reference signals in the m-th system. Several scenarios, characterized by different number of multi-path components, power profiles (PP), and Delay Profiles (DP) are considered for the dual-band system (Table 3.2). These

SAGE			
Delay sampling interval [s]		1×10^{-10}	
Termination threshold γ_τ		1×10^{-4}	
Maximum number of iterations $i_{\max}$		100	
Number of symbols		1000	
Dual-band		**Equivalent single-band**	
N_1, N_2	2048	$N = N_1 + N_2$	4096
$N_{\mathrm{cp}_1}, N_{\mathrm{cp}_2}$	144	$N_{\mathrm{cp}} = N_{\mathrm{cp}_1} + N_{\mathrm{cp}_2}$	288
$N_{\mathrm{u}_1}, N_{\mathrm{u}_2}$	1200	$N_{\mathrm{u}} = N_{\mathrm{u}_1} + N_{\mathrm{u}_2}$	2400
$N_{\mathrm{s}_1}, N_{\mathrm{s}_2}$	200	$N_{\mathrm{s}} = N_{\mathrm{s}_1} + N_{\mathrm{s}_2}$	400
Δf [kHz]	15	Δf [kHz]	15
f_{c_1} [MHz]	1835	$f_c = f_{c_1}$ [MHz]	1835
f_{c_2} [MHz]	1855		

Table 3.1: Parameters and settings.

scenarios have been specifically selected to represent increasingly complex situations for the purposes of LoS ToA estimation.

The first set of results, reported in Fig. 3.1, shows the RMSE performance for $L = 2$ as a function of the Signal-to-Noise Ratio (SNR). To quantify the possible benefits, the derived performance is compared to that obtained by two single-band systems: a first one using half of the bandwidth, and a second one using the entire bandwidth (equivalent single-band). We may observe from this figure that the dual-band ToA estimation is better than the half-bandwidth single-band one, and is close to the equivalent single-band estimation especially in low SNR conditions. It is hence worth going on to check the performance of the dual-band system in a wider set of scenarios.

L		2	
PP [dB]		[0 0]	
Scenario		Band 1	Band 2
1	DP [μs]	$[1, 1.1]$	$[1.05, 1.15]$
L		4	
PP [dB]		[0 -2 -10 -20]	
Scenario		Band 1	Band 2
1	DP [μs]	$[1, 1.2, 1.4, 1.6]$	$[1, 1.2, 1.4, 1.6]$
2	DP [μs]	$[1, 1.2, 1.4, 1.6]$	$[1, 1.2, 1.4, 1.8]$
3	DP [μs]	$[1, 1.2, 1.4, 1.6]$	$[1, 1.2, 1.6, 1.8]$
4	DP [μs]	$[1, 1.2, 1.4, 1.6]$	$[1, 1.4, 1.6, 1.8]$
L		6	
PP [dB]		[0 -4 -8 -12 -16 -20]	
Scenario		Band 1	Band 2
1	DP [μs]	$[1, 1.1, 1.2, 1.3, 1.4, 1.5]$	$[1, 1.1, 1.2, 1.3, 1.4, 1.5]$
2	DP [μs]	$[1, 1.1, 1.2, 1.3, 1.4, 1.5]$	$[1, 1.1, 1.2, 1.3, 1.6, 1.7]$
3	DP [μs]	$[1, 1.1, 1.2, 1.3, 1.4, 1.5]$	$[1, 1.1, 1.4, 1.5, 1.6, 1.7]$
4	DP [μs]	$[1, 1.1, 1.2, 1.3, 1.4, 1.5]$	$[1, 1.3, 1.4, 1.5, 1.6, 1.7]$

Table 3.2: Simulated dual-band scenarios.

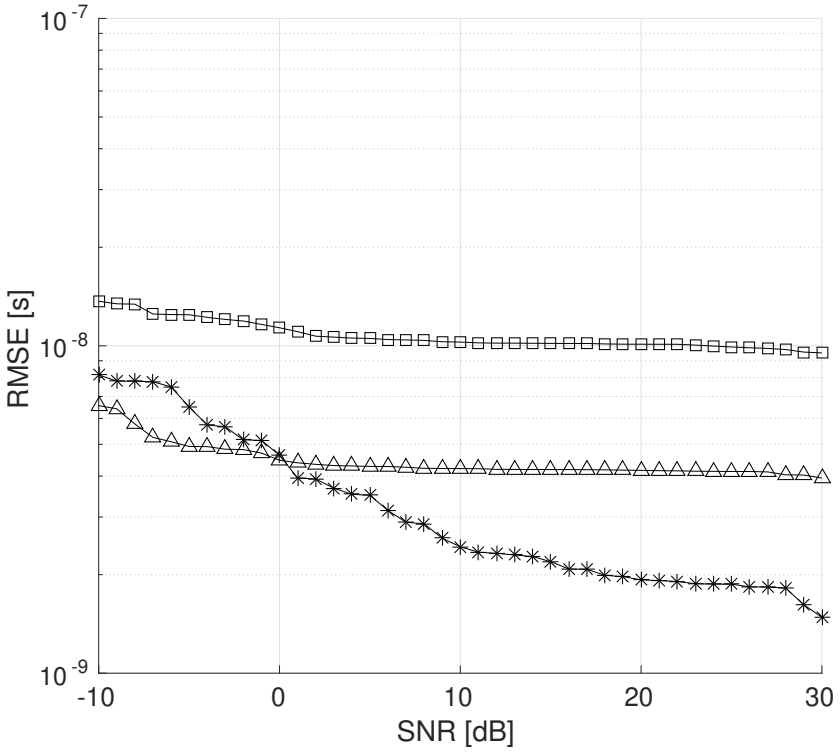

Figure 3.1: SAGE ToA estimation for scenario 1 with $L = 2$. $\square$: Single-band $\triangle$: Dual-band $*$: Equivalent single-band.

This is the objective of the simulations that lead to Fig. 3.2 and Fig. 3.3, which reports the ToA RMSE performance in different scenarios for $L = 4$ and $L = 6$ respectively.

With reference to Fig. 3.2, a direct comparison between a single-band and a dual-band system shows that the latter presents a lower RMSE in low SNR conditions. This behavior is due to the fact that, at low SNRs, the main impact on the estimation error is determined by the noise, which partly hides the inaccurate estimation of the secondary path. Instead, at high SNRs, this inaccuracy becomes dominant in higher-order scenarios. However, as the multi-path environment becomes richer ($L = 6$), the dual-band system tends

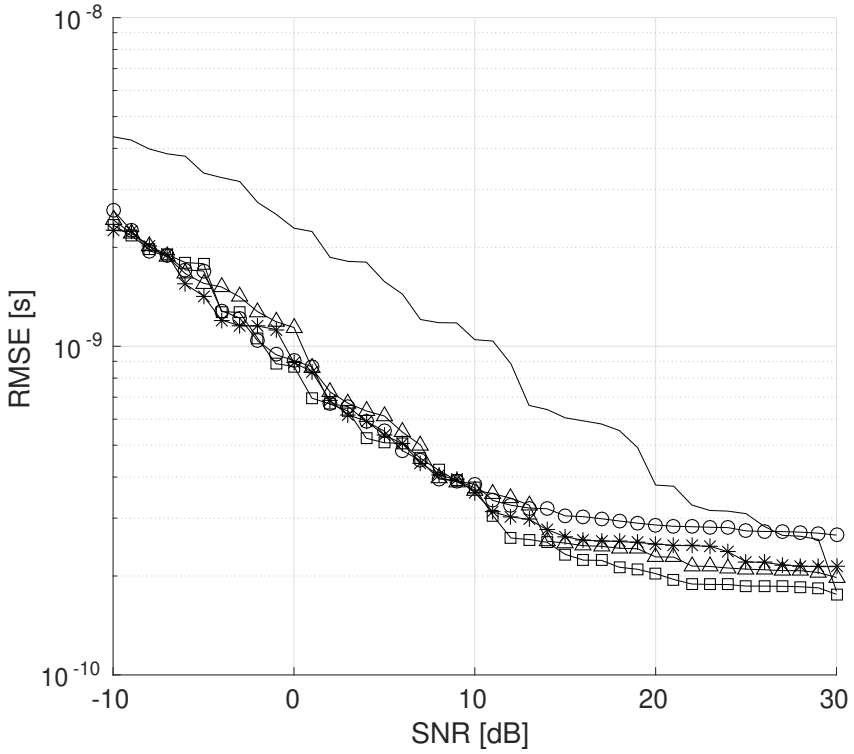

Figure 3.2: SAGE ToA estimation for scenarios with $L = 4$. $-$: Single-band $\square$: Dual-band (scenario 1) $\triangle$: Dual-band (scenario 2) $*$: Dual-band (scenario 3) $\circ$ Dual-band (scenario 4).

to outperform the single-band one even in high SNR conditions.

A general aspect that can be highlighted regarding this second set of results concerns the negative influence of the inaccuracy in estimating the delays of the secondary paths on the estimation of the ToA referred to the LoS one, even if it has been assumed identical on the two bands in all the analyzed scenarios. In summary, however, the above results suggest that a dual-band OFDM system might be usefully exploited for ToA estimation purposes when the power-delay profiles of the two bands are correlated enough.

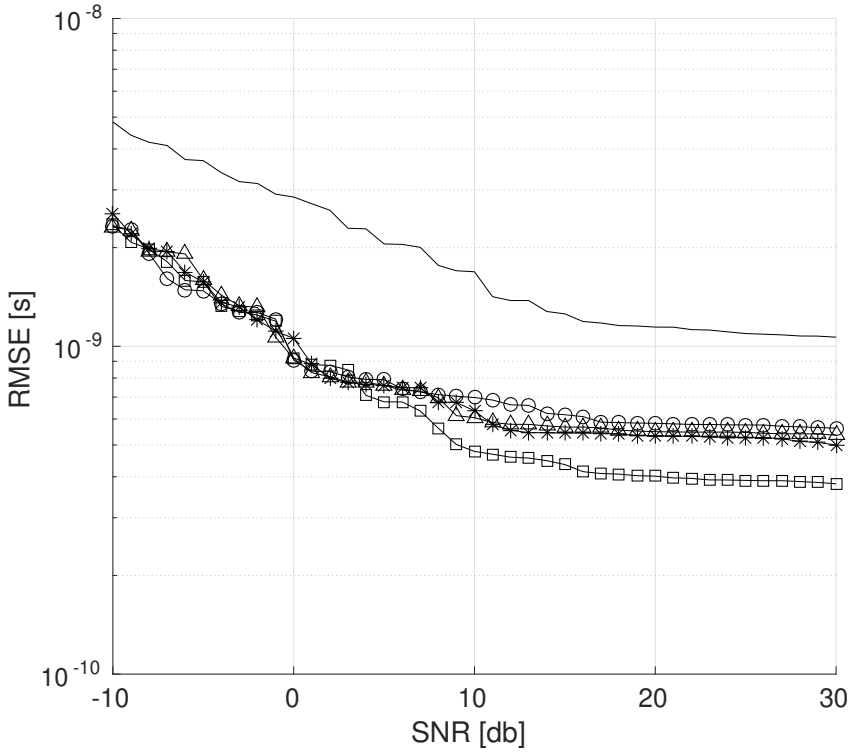

Figure 3.3: SAGE ToA estimation for scenarios with $L = 6$. $-$: Single-band $\square$: Dual-band (scenario 1) $\triangle$: Dual-band (scenario 2) $*$: Dual-band (scenario 3) $\circ$ Dual-band (scenario 4).

3.3 Multi-Band SAGE Application

The use of the SAGE in multiple-bands scenarios has been investigated, with the purpose of combining information coming from non-synchronized transmission bands.

A different implementation of the SAGE algorithm was selected for the investigation. The chosen implementation of SAGE, derived from [54] and [55], differs substantially from the one of Section 3.2.1 as described in the following section.

3.3.1 SAGE Implementation

Initialization The initial parameter vector $\boldsymbol{\theta}(-L+1)$ is set to 0. This means that the first iteration of the algorithm is completely blind, as only the parameters for the waves already detected are exploited in the E-step. The notation indicates that the first L iterations of the algorithm are necessary to fully initialize it before the actual SAGE iteration can start.

E-step As in the EM algorithm, interference cancellation is performed to isolate the contribution of the l-th path. The initial L iterations however differ from the regular ones. During the initialization phase this is performed with Serial Interference Cancellation (SIC), as only the parameters relative to the paths that have already been detected are cancelled:

$$\bar{H}_l(f_k, t_s) = \bar{H}(f_k, t_s) - \sum_{l'=1}^{i-1} H_{l'}(f_k, t_s; \hat{\boldsymbol{\theta}}'_{l'}) \tag{3.13}$$

where i is the current iteration of the SAGE algorithm. In the iterations of the algorithm after the L-th, the Expectation step is carried out as described in Section 3.1.1.

M-step During the Maximization step, the parameters relative to a single path are updated sequentially, based on the previous estimates. Each parameter is updated separately by solving a single-dimensional maximization problem.

$$\hat{\tau}''_l = \arg\max_{\tau} \left\{ \left| z\left(\tau, \hat{\phi}'_l, \hat{f}'_{D,l}; \hat{H}_l(f_k, t_s)\right) \right| \right\} \tag{3.14a}$$

$$\hat{\phi}''_l = \arg\max_{\phi} \left\{ \left| z\left(\tau''_l, \phi, \hat{f}'_{D,l}; \hat{H}_l(f_k, t_s)\right) \right| \right\} \tag{3.14b}$$

$$\hat{f}''_{D,l} = \arg\max_{f_D} \left\{ \left| z\left(\tau''_l, \hat{\phi}''_l, f_D; \hat{H}_l(f_k, t_s)\right) \right| \right\} \tag{3.14c}$$

where z is the correlation function. The amplitude $\hat{\alpha}_l$ is then updated as per (3.7)

3.3.2 Methods for Multi-Band SAGE Application

The multi-band ToA estimation method is developed building upon the SAGE algorithm as described in Section 3.3.1. Let $\mathcal{K}_{\mathrm{R},m} \subseteq \mathcal{K}_m$ be the set of sub-carrier frequencies, equally spaced by $\Delta f_{\mathrm{R},m}$, for which a CFR sample is available for the m-th OFDM sub-system. Equivalently, $\mathcal{K}_{\mathrm{R},m}$ is the set of sub-carriers occupied by exploitable reference symbols in the m-th OFDM sub-system. Also let $\mathcal{T}_{\mathrm{o},m}$ be the set of time instants when the CFR is sampled for the m-th sub-system. The overall set of observed CFR samples for sub-band m is denoted as $\bar{H}_m(k,t)$, $k \in \mathcal{K}_{\mathrm{R},m}$, $t \in \mathcal{T}_{\mathrm{o},m}$.

At this point two assumptions are introduced. First, the CFR observations are taken at the same time instants for all the sub-bands, that is, $\mathcal{T}_{\mathrm{o},m} = \mathcal{T}_{\mathrm{o}}$, $m = 1, \ldots M$. Even if the reference symbols are not synchronized between the transmitters, it is sufficient that the time offset between corresponding symbols is smaller than the coherence time of the channel. Second, the number of pilot tones N_{R} and their frequency spacing $\Delta f_{\mathrm{R},m}$ are assumed to be uniform across all sub-systems, that is, $\Delta f_{\mathrm{R},m} = \Delta f_{\mathrm{R}}$, $m = 1, \ldots M$.

From this point on, only the $m = 2$ (dual-band) case will be considered, being the extension to the $m > 2$ case straightforward.

SAGE receives as input a time-frequency matrix $\bar{H}(f,t)$ of contiguous CFR samples, as shown in Fig. 3.4. The available samples for the transmission bands $\bar{H}_m(f,t)$ must hence be joined into a single time-frequency matrix $\bar{H}_T(f,t)$ that is used as input for the SAGE algorithm.

However, base stations generally lack synchronization between the clocks of the transmitters, meaning that additional processing is needed before the

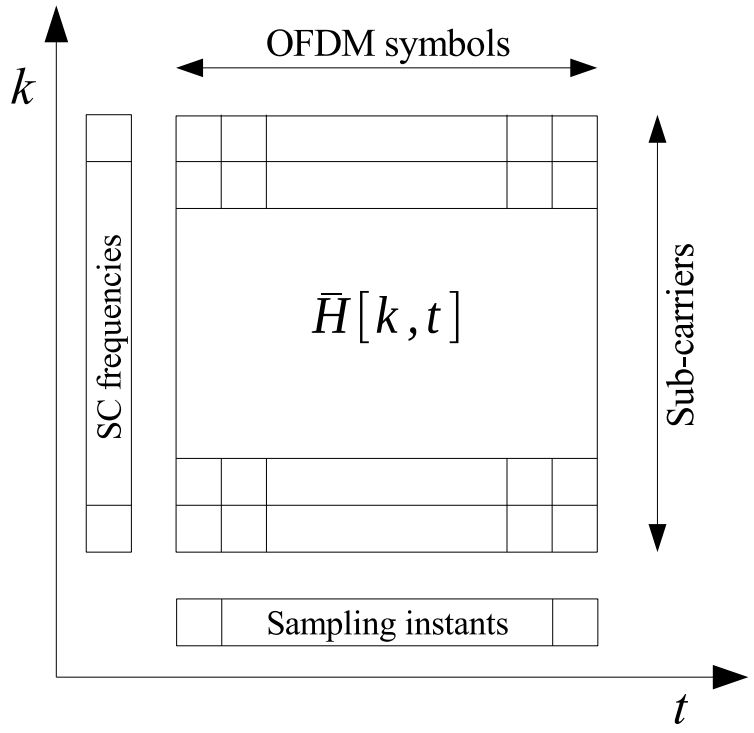

Figure 3.4: The time-frequency CFR estimation matrix.

information from the two sub-bands can be combined. In [56] a method is proposed to synchronize the downlink signals of LTE base stations for ranging purposes. In most current network deployments, however, LTE base stations are asynchronous. To this end, two methods are introduced: Signal Combining and Signal Aggregating.

3.3.3 Signal Combining

In the Signal Combining technique, Maximal Ratio Combining is used to combine the available estimations. The algorithm consists of an initialization part, in which the timing offset between the two transmission bands is estimated, and a main part in which data from the two bands are combined to achieve a ToA estimation.

The set of CFR sampling instants $\mathcal{T}_{\mathrm{o}}$ is subdivided in a number Q of adjacent sub-sets t_q, each containing N_{t} contiguous elements so that:

$$\mathcal{T}_{\mathrm{o}} = \bigcup \mathrm{t}_q \quad q = 1, \ldots, Q \tag{3.15}$$

Correspondingly, the CFR samples for each transmission band are subdivided in sub-sets $\hat{H}_m^q(f,t)$, $f \in \mathcal{K}_{\mathrm{R},m}$, $t \in \mathrm{t}_q$ of N_{t} time-contiguous CFR estimations spanning the available bandwidth of each sub-system.

Initialization 1 The SAGE algorithm is applied separately to the first chunk of data from each transmission band, $\hat{H}_1^1(f,t)$ and $\hat{H}_2^1(f,t)$ respectively, resulting in the estimated parameters $\hat{L}_1$, $\hat{\tau}_l^{(1)}$ and $\hat{\sigma}_{n,1}^2$ for Band 1 and $\hat{L}_2$, $\hat{\tau}_l^{(2)}$ and $\hat{\sigma}_{n,2}^2$ for Band 2. Because of the lack of synchronization between the two transmitters, the ToA of the two signals will not be the same. The timebase of the first signal is arbitrarily chosen as reference.

Initialization 2 The time shift is calculated as:

$$t_{\mathrm{s}} = \hat{\tau}_1^{(2)} - \hat{\tau}_1^{(1)} \tag{3.16}$$

The signal-combining ToA estimation algorithm is then applied for each of the Q pair of samples sub-sets $\hat{H}_1^q(f,t)$ and $\hat{H}_2^q(f,t)$.

Step 1 By substituting $\phi_s = 2\pi\Delta f_R t_{\mathrm{s}}$, the phase-shifting matrix is defined as:

$$\Phi_{\mathrm{s}} = \begin{bmatrix} e^{-j\phi_s} & e^{-j\phi_s} & \ldots & e^{-j\phi_s} \\ e^{-j2\phi_s} & e^{-j2\phi_s} & \ldots & e^{-j2\phi_s} \\ \vdots & \vdots & & \vdots \\ e^{-jN_{\mathrm{R}}\phi_s} & e^{-jN_{\mathrm{R}}\phi_s} & \ldots & e^{-jN_{\mathrm{R}}s\phi_s} \end{bmatrix} \tag{3.17}$$

where Δf_R is the frequency spacing between reference signals. This accounts for the clock shift between the two transmitters.

Step 2 An additional phase shift is added to account for the carrier phase. Hence, by substituting;

$$\phi_c = \min\left[\mathcal{K}_{\mathrm{R},2}\right] t_{\mathrm{s}} + (f_{C,2} - f_{C,1})\hat{\tau}_1^{(2)} \tag{3.18}$$

where $f_{C,1}$ and $f_{C,2}$ are the carrier frequencies for Band 1 and Band 2 respectively. The second phase-shifting matrix is defined as:

$$\Phi_{\mathrm{sc}} = e^{-j2\pi\phi_c} \cdot 1_{N_{\mathrm{R}} \times N_{\mathrm{t}}} \tag{3.19}$$

where $1_{m\times n}$ is a $m \times n$ matrix of ones. The shifts are then applied to Band 2 by phase-shifting the CFR estimation matrix:

$$\tilde{H}_2^q = \hat{H}_2^q \otimes \Phi_{\mathrm{s}} \otimes \Phi_{\mathrm{sc}} \tag{3.20}$$

where $\otimes$ denotes the elementwise product between matrices.

Step 3 Weighed signal combining is performed. By substituting $d_\sigma = \frac{1}{\hat{\sigma}_{n,2}^2} - \frac{1}{\hat{\sigma}_{n,1}^2}$, the combined input matrix is calculated as:

$$\hat{H}_{\mathrm{C}}^q = \hat{H}_1^q + 10^{d_\sigma/20}\tilde{H}_2^q \tag{3.21}$$

Step 4 The SAGE algorithm is applied to $\hat{H}_{\mathrm{C}}^q$, resulting into the final estimations $\hat{L}_{\mathrm{C}}$ and $\hat{\tau}_{l,\mathrm{C}}$.

For the Signal Combining method to be used efficiently, the propagation environment must be highly correlated between the two sub-bands. If not, the combined CFR values might lead to bias in the estimation of the ToA of the first path.

3.3.4 Signal Aggregating

In Signal Aggregating, the estimated CFR matrices are joined into a larger matrix. Usually a guard band is inserted between the transmission bands

of a multi-band OFDM system, to avoid interference and ease the filtering operations at the receiver. Hence, zero filling is needed to fill the frequency gap between the available CFR samples. The added zeros do not affect the outcome of the estimation and allow the use of an efficient implementation of the SAGE algorithm. Similar to Signal Combining, the available CFR samples are subdivided in a number Q of sub-sets and the time shift between the transmission bands is estimated with a first run of SAGE.

Initialization Similarly to the Signal Combining method, the SAGE algorithm is applied separately to the first chunk of data from each transmission band and the time shift is calculated as per (3.16).

Step 1 The phase-shifting matrix is defined as per (3.17). Because the samples are aggregated instead of added together, the difference in carrier frequency is naturally accounted for by the SAGE implementation.

Step 2 A further shift ϕ_a is needed to compensate the effects of the timing offset.

$$\phi_a = \min\left[\mathcal{K}_{\mathrm{R},2}\right] t_{\mathrm{s}} \tag{3.22}$$

The additional phase-shifting matrix is defined as:

$$\Phi_{\mathrm{sa}} = e^{-j2\pi\phi_a} \cdot 1_{N_{\mathrm{R}} \times N_{\mathrm{t}}} \tag{3.23}$$

The shifts are then applied to Band 2 by phase-shifting the CFR estimation matrix:

$$\tilde{H}_2^q = \hat{H}_2^q \otimes \Phi_{\mathrm{s}} \otimes \Phi_{\mathrm{sa}} \tag{3.24}$$

Step 3 The CFR matrices are aggregated and zeros are added to fill the frequency gap. Being:

$$f_{\mathrm{gap}} = \min\left[\mathcal{K}_{\mathrm{R},2}\right] - \max\left[\mathcal{K}_{\mathrm{R},1}\right] \tag{3.25}$$

the frequency gap between the two bands, a number $N_{\mathrm{G}} = \lfloor f_{\mathrm{gap}}/\Delta f_R \rfloor$ of null sub-carriers is inserted to account for the gap.

$$\hat{H}^q_{\mathrm{A}} = \begin{bmatrix} \hat{H}^q_1 & 0_{N_{\mathrm{t}} \times N_{\mathrm{G}}} & \tilde{H}^q_2 \end{bmatrix} \tag{3.26}$$

where $0_{m \times n}$ is a $m \times n$ null matrix.

Step 4 The SAGE algorithm is applied to $\hat{H}^q_{\mathrm{A}}$, resulting into the final estimations $\hat{L}_{\mathrm{A}}$ and $\hat{\tau}_{l,\mathrm{A}}$.

4 Simulated Results

This section discusses the results obtained from simulations for multi-band estimation using the Signal Combining and Signal Aggregating methods proposed in Section 3. Simulations have been run to assess the behavior of the SAGE-based methods in multi-path propagation environments. The considered LTE scenario uses the CRS as the reference signal to simulate real-life measurements as closely as possible.

4.1 Overview of Simulations

Simulations were used to investigate the behavior of multi-band methods in complex propagation scenarios. The simulator is designed to accurately implement the LTE downlink layer signals. Assuming that the propagation environment doesn't change over the duration of a single LTE slot, it is possible to merge the $s = 0$ and $s = 4$ reference symbols of a slot into a single OFDM symbol with twice as many REs occupied by CRS tones. This merged symbol is considered to be transmitted once per slot at $s = 0$, and the spacing between pilot tones becomes half the normal one, that is, $\Delta f_{\text{CRS}} = 3\Delta f = 45$ kHz. This is shown in Fig. 4.1. As such, each LTE slot corresponds to a merged reference symbol. Because $N_{\text{t}} = 20$ consecutive pilot symbols are grouped together, a SAGE estimation output is obtained each 20 symbols, equivalent to a LTE frame of data.

The parameters adopted for the simulations are reported in Table 4.1, where N is the number of sub-carriers occupied by modulated symbols and N_{R} is the number of sub-carriers reserved for reference symbols. These values have been chosen to mirror the scenario encountered during the live measurement campaign as closely as possible. Both algorithms have been simulated using the same parameter values.

The metrics chosen to evaluate the performance are the RMSE, range r_τ, and standard deviation σ_τ of the estimated ToA values.

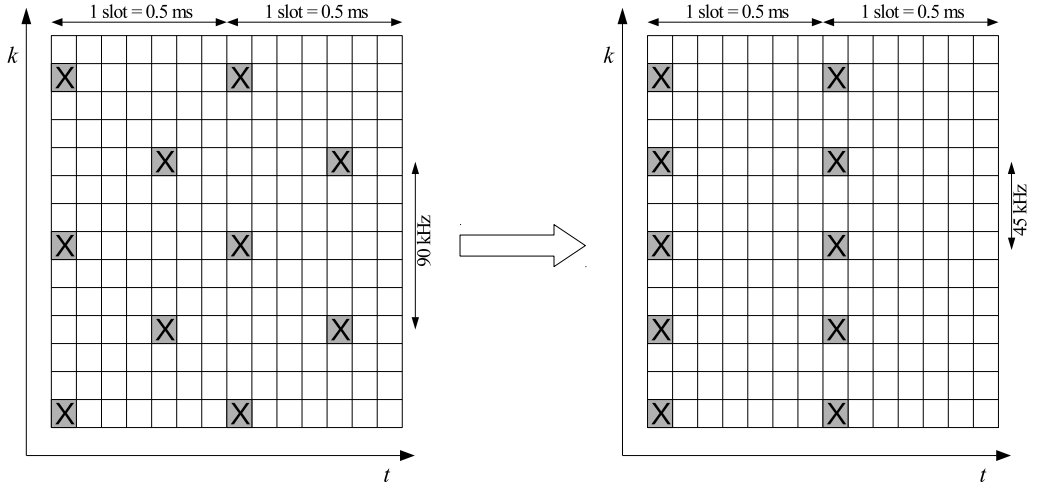

Figure 4.1: CRS merging over a single LTE slot.

$L = 4$		
PP [dB]	[0 -2 -10 -20]	
	Band 1	Band 2
DP [μs]	$[1, 1.2, 1.4, 1.6]$	$[1.1, 1.3, 1.5, 1.7]$
$L = 6$		
PP [dB]	[0 -4 -8 -12 -16 -20]	
	Band 1	Band 2
DP [μs]	$[1, 1.1, 1.2, 1.3, 1.4, 1.5]$	$[1.1, 1.2, 1.3, 1.4, 1.5, 1.6]$
SNR [dB]	$-10 \div 30$	
BW [MHz]	10	
N	600	
N_{R}	200	
N_{t}	20	
N_{symb}	1000	

Table 4.1: Simulated dual-band scenarios.

4.2 Simulations - Signal Combining

4.2.1 Performance Assessment

The Signal Combining method is simulated over the channel models of Table 4.1 to assess its performance in a multi-path propagation environment.

The simulated results for the 4-paths channel model (based on the COST207 RA4 specifications) are shown in Fig. 4.2. This propagation model presents a strong second path and a wide delay spread. The Signal Combining method achieves a moderate performance gain across the considered SNR range when compared to single-band estimation. Figs. 2(a)-2(c) display a common trend for the three considered metrics.

The channel model considered for the results of Fig. 4.3 is based on the COST207 RA6 6-paths specifications. In this case Signal Combining presents no performance gain at low-to-mid SNR values when compared to single-band estimation, while at higher SNR values the dual-band estimation method shows better performance. This behavior is displayed for all the considered performance metrics (Figs. 3(a)-3(c)).

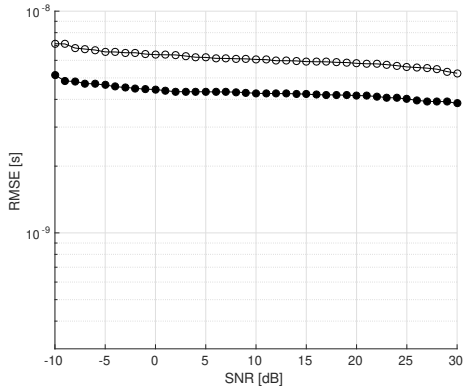

(a) RMSE performance.

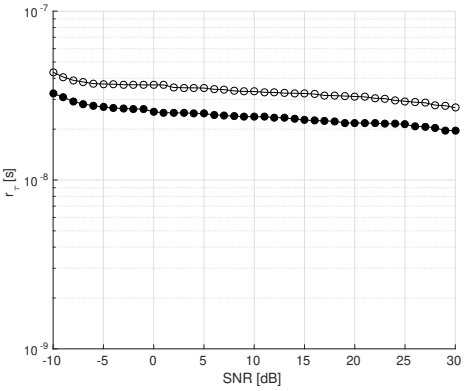

(b) Range performance.

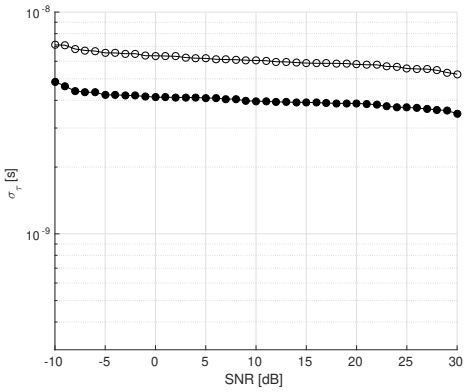

(c) Std. dev. performance.

Figure 4.2: Performance metrics for the Signal Combining method for the $L = 4$ scenario. ○: Single-band estimation ●: Dual-band estimation.

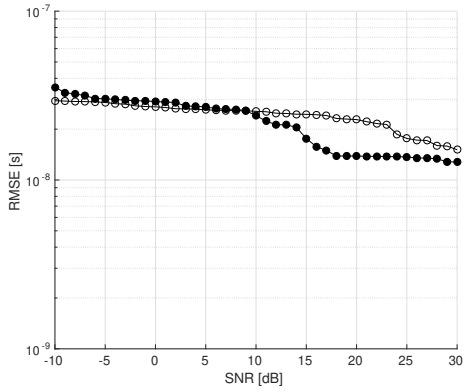

(a) RMSE performance.

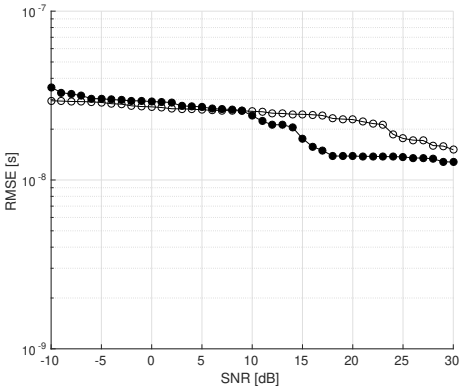

(b) Range performance.

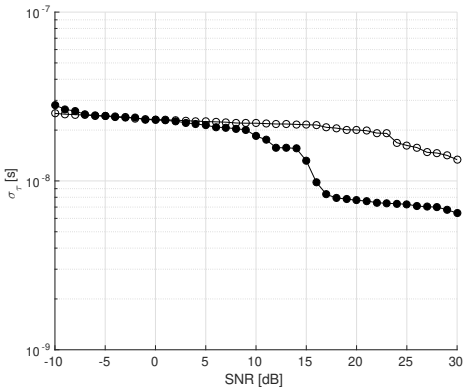

(c) Std. dev. performance.

Figure 4.3: Performance metrics for the Signal Combining method for the $L = 6$ scenario. ○: Single-band estimation ●: Dual-band estimation.

4.2.2 Example Estimation

Two examples of ToA estimation performed using the Signal Combining method are shown in Fig. 4.4 and Fig. 4.5. The figures refer to a time span of 50 LTE frames, corresponding to the 500 ms duration of real-life measurements, and a SNR of 0 dB in both the transmission bands.

Table 4.2 and Table 4.3 summarize the performance metrics for the scenarios. Confirming the trend of 4.2.1, in both the considered cases the range r_τ and standard deviation σ_τ decrease significantly when both transmission bands are employed for estimation. The RMSE is also noticeably smaller in the dual-band case.

The estimated ToA values reported in Figs. 4.4-4.5 are normalized to the value of the first path ToA (1 μs in the simulations), to allow a more immediate comparison of the range and spread of the estimation sets.

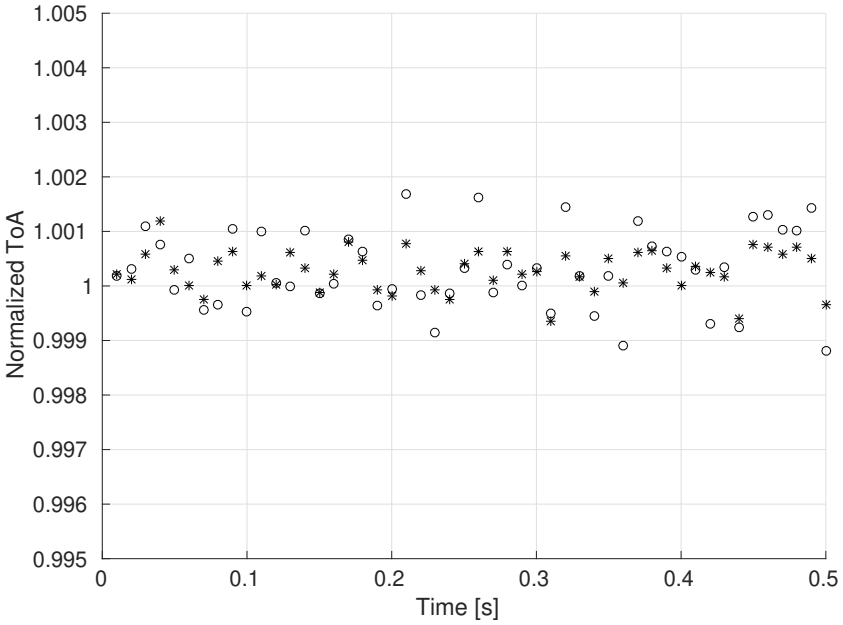

Figure 4.4: Normalized ToA estimation simulation with the Signal Combining method for the $L = 4$ scenario. $\circ$: Single-band estimation $*$: Dual-band estimation.

$L = 4$		
SNR [dB]	0	
	Single-Band	Dual-Band
r_τ [ns]	2.879	1.852
σ_τ [ns]	0.716	0.373
RMSE [ns]	2.195	1.942

Table 4.2: Simulated performance for the Signal Combining method for the $L = 4$ scenario.

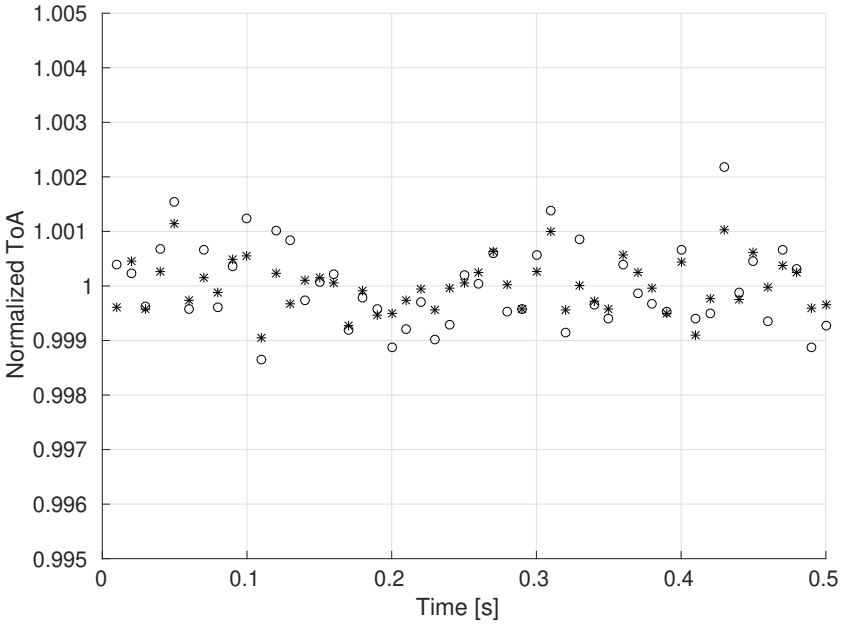

Figure 4.5: Normalized ToA estimation simulation with the Signal Combining method for the $L = 6$ scenario. $\circ$: Single-band estimation $*$: Dual-band estimation.

$L = 6$		
SNR [dB]	0	
	Single-Band	Dual-Band
r_τ [ns]	3.543	2.085
σ_τ [ns]	0.748	0.466
RMSE [ns]	0.851	0.482

Table 4.3: Simulated performance for the Signal Combining method for the $L = 6$ scenario.

4.3 Simulations - Signal Aggregating

4.3.1 Performance Assessment

The simulated performance of the Signal Aggregating method can be seen in Fig. 4.6 and Fig. 4.7 for the $L = 4$ and $L = 6$ propagation scenarios respectively.

The Signal Aggregating method shows a large performance gain in both the considered scenarios. The gain obtained with the use of the added bandwidth results much greater than the one achieved by Signal Combining.

It can also be observed in the $L = 6$ scenario that the performance of the dual-band estimation presents an almost flat behavior across the considered SNR range, whereas single-band estimation metrics decrease as the SNR increases.

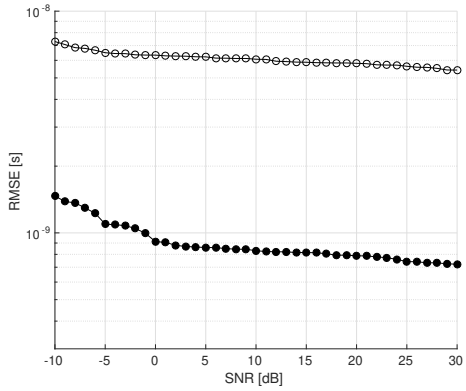

(a) RMSE performance.

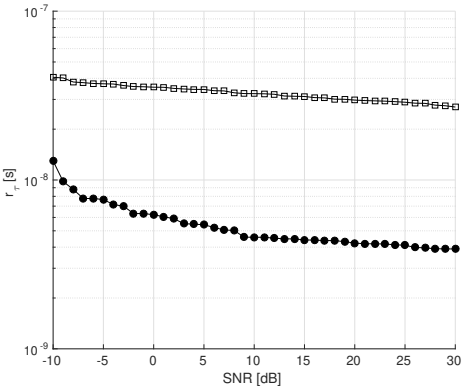

(b) Range performance.

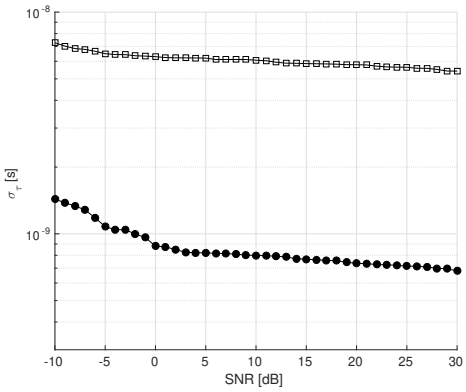

(c) Std. dev. performance.

Figure 4.6: Performance metrics for the Signal Aggregating method for the $L = 4$ scenario. ○: Single-band estimation ●: Dual-band estimation.

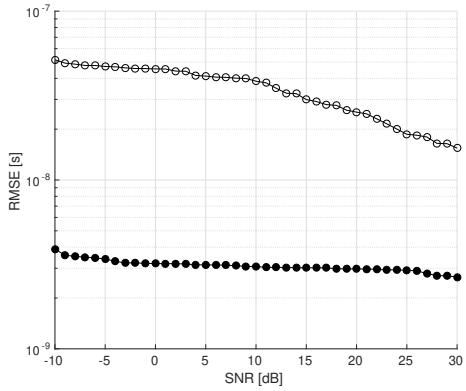

(a) RMSE performance.

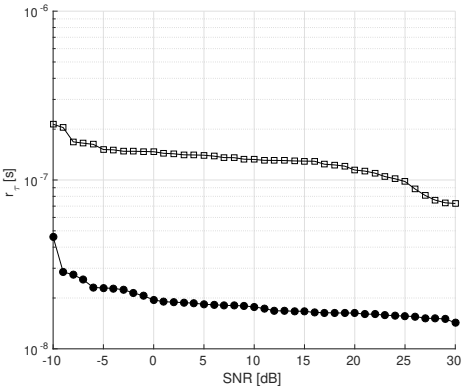

(b) Range performance.

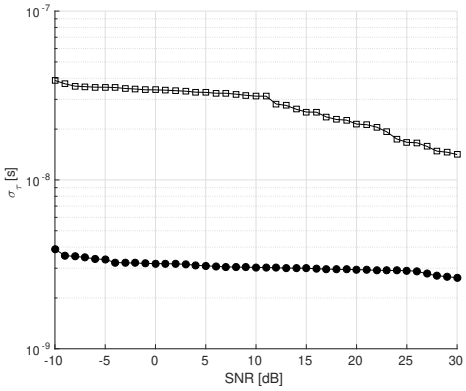

(c) Std. dev. performance.

Figure 4.7: Performance metrics for the Signal Aggregating method for the $L = 6$ scenario. ○: Single-band estimation ●: Dual-band estimation.

4.3.2 Example Estimation

Examples of simulated estimation employing the Signal Aggregating method are shown in Fig. 4.8 and Fig. 4.9. The COST207 RA4 4-paths and COST207 RA6 6-paths channel models are considered. The SNR for both transmission band is 0 dB. The simulated performance are reported in Table 4.4 and Table 4.5. Agreeing with the previous results, the Signal Aggregating method achieves better performance than Signal Combining at the cost of a slightly larger computational complexity because of the larger size of the SAGE algorithm input matrix. Table 4.4 and Table 4.5 summarize the metrics obtained from the simulations. As per the Signal Combining method, the reported ToA values are normalized to the value of the first path ToA for comparison purposes.

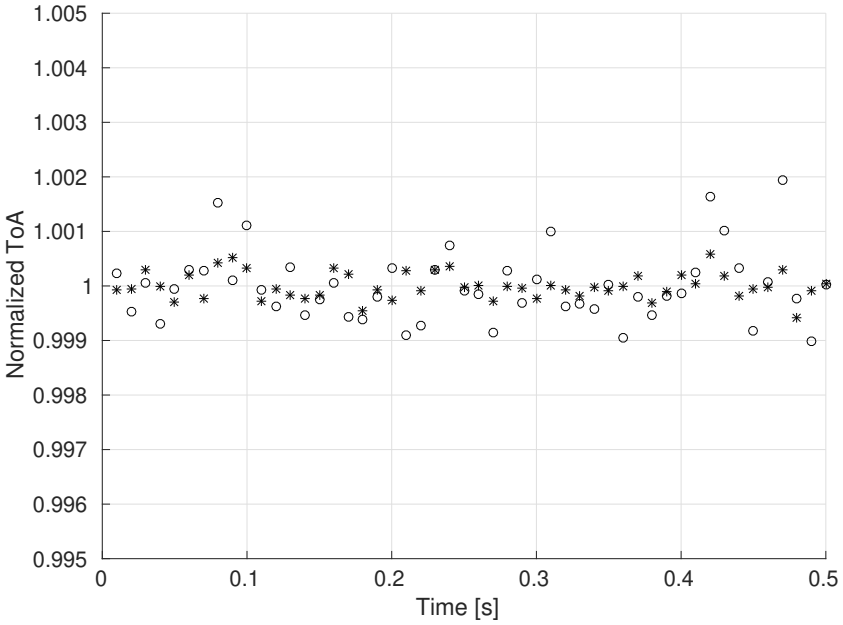

Figure 4.8: Normalized ToA estimation simulation with the Signal Aggregating method for the $L = 4$ scenario. $\circ$: Single-band estimation $*$: Dual-band estimation.

$L = 4$		
SNR [dB]	0	
	Single-Band	Dual-Band
r_τ [ns]	2.958	1.154
σ_τ [ns]	0.648	0.244
RMSE [ns]	2.326	0.201

Table 4.4: Simulated performance for the Signal Aggregating method for the $L = 4$ scenario.

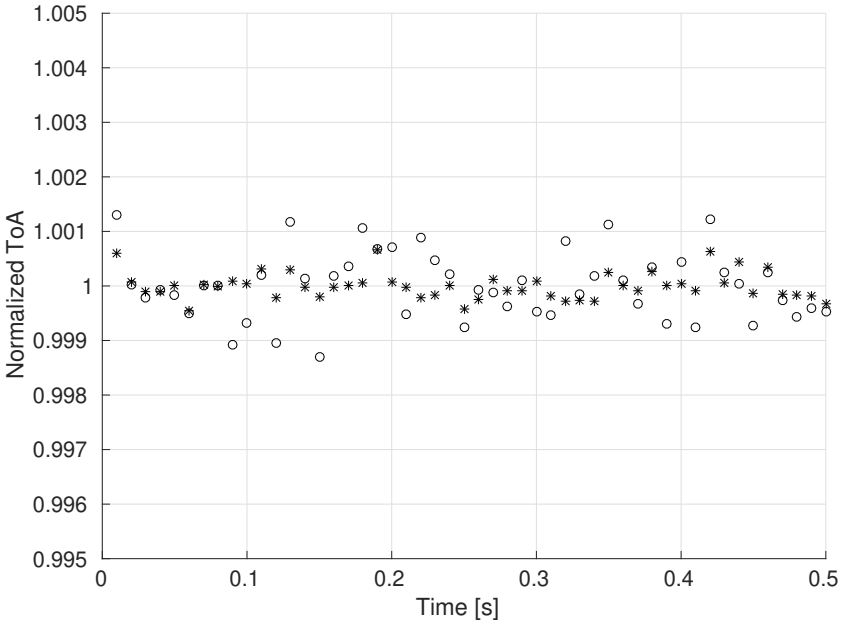

Figure 4.9: Normalized ToA estimation simulation with the Signal Aggregating method for the $L = 6$ scenario. $\circ$: Single-band estimation $*$: Dual-band estimation.

$L = 6$		
SNR [dB]	0	
	Single-Band	Dual-Band
r_τ [ns]	2.605	1.117
σ_τ [ns]	0.618	0.246
RMSE [ns]	1.129	0.667

Table 4.5: Simulated performance for the Signal Aggregating method for the $L = 6$ scenario.

5 Measurements Setup and Scenario

In this chapter the measurement campaign for the real-time acquisition of LTE downlink signals is illustrated. The CellSearch LTE scan tool was employed in the search for a suitable Base Station carrying multiple transmitters, as it provides a cheap and easily portable tool for scanning the surrounding LTE cells. To obtain usable measurements of the LTE signal, instrumentation that provides high-frequency sampling and synchronized acquisitions is needed. The scenario in which the measurements have been taken is also presented, together with the configuration of the transmitting base station.

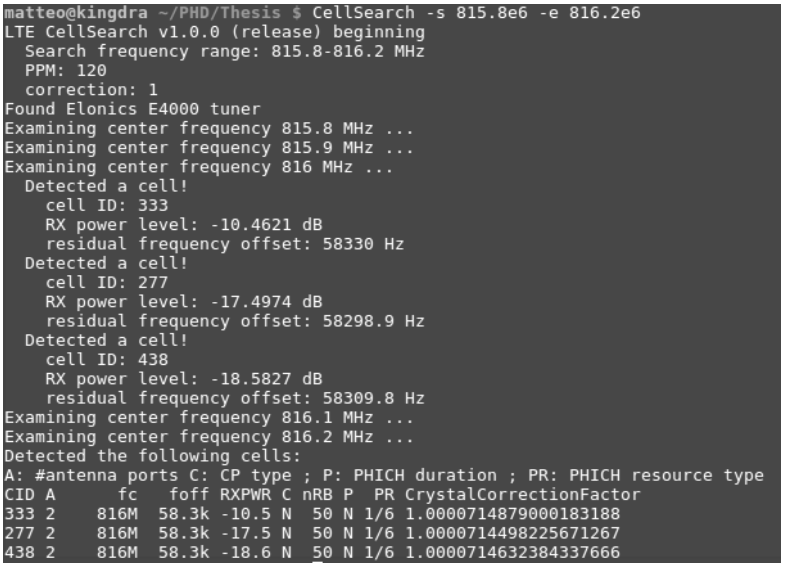

Figure 5.1: Example screenshot of the CellSearch scan tool.

5.1 The CellSearch scan tool

The LTE Cell Scanner software tool is used to locate LTE BS cells using very low performance RF front ends. This tools operates with USB dongles based on the RTL2832 tuner chip. The RTL2832 tuner chip has a noise figure of 20 dB, a 8 bits ADC, and an oscillator crystal with a frequency error of about 100 ppm.

The CellSearch tool can be used to search for LTE carriers within a specified range of frequencies. It outputs a number of parameters for the detected cell IDs, including the received power, frequency offset, and the cell configuration. An example output is shown in Fig. 5.1. The tool is available for free from [57] and can run on any reasonably modern Linux distribution.

5.2 Instrumentation Setup

The measurements setup comprises two Universal Radio Peripheral (USRP) Ettus N210 Software Defined Radios (SDR) [58]. The block scheme of the instrumentation setup is shown in Fig. 5.2. The two USRP SDRs are employed to simultaneously measure two channels, in the considered scenario two downlink signals from different operators allocated on the same base station mast. The Ettus USRP Network Series offers high-bandwidth, high-dynamic range processing capability and MIMO capabilities. The Gigabit Ethernet interface of the USRP Network Series allows high-speed streaming capability up to 50 millions of samples per second (MSPS) in both directions when the 8-bit samples configuration is used. These features, combined with plug-and-play MIMO capability make the USRP Network an ideal candidate for software defined radio systems with demanding performance requirements. The USRP mounted a WBX daughterboard, which has a frequency capability range from 50 to 2200 MHz and a maximum noise figure of 5 dB.

A high-precision 10 MHz reference clock from a GPS-locked SRS FS 725 Rubidium frequency standard is employed to synchronize the two USRPs. Both USRP units are connected to the 10 MHz reference clock, so the data acquisition is synchronized between the two units. A u-blox EVK-6N GNSS evaluation kit provides the GPS-locked PPS signal to the Rubidium clock. The GNSS module employs a magnetic-mount vehicular antenna.

A conventional personal computer (PC) acts as system controller and data recording unit, guaranteeing coherent sampling between the two USRP devices. The PC is connected to the USRP units via Gigabit Ethernet connections. The calculator presents a separate GbE interface for each of the connected USRPs, so each unit can make use of the full 1 Gb data rate.

Labview is used as the data acquisition software, allowing for easy config-

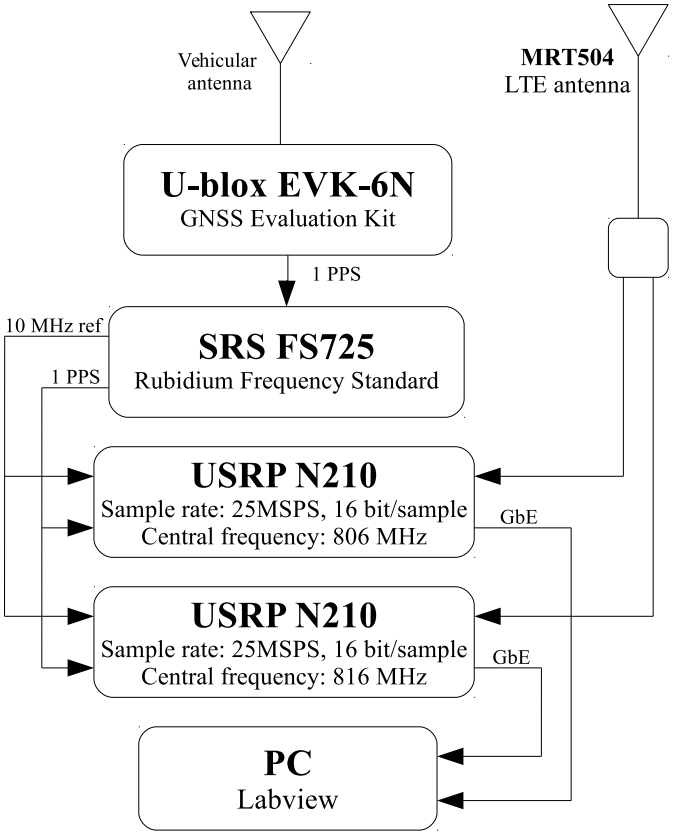

Figure 5.2: Block scheme of the measurement setup.

uration and synchronization between the two USRP units. Data is recorded in a binary format, with a sampling rate of 25 MSPS and a precision of 16 bits for the real and imaginary part of each sample. The acquisition scheme has been developed by Alessandro Pin from University of Udine.

A single directive MRT504 LTE wide-band antenna is used, coupled with a two-way splitter to feed the signal to the two USRP measuring units.

5.3 Measurement Scenario

The dual-band measurements have been performed in Monfalcone, Italy, in an industrial district characterized by low-rise buildings and parking lots sep-

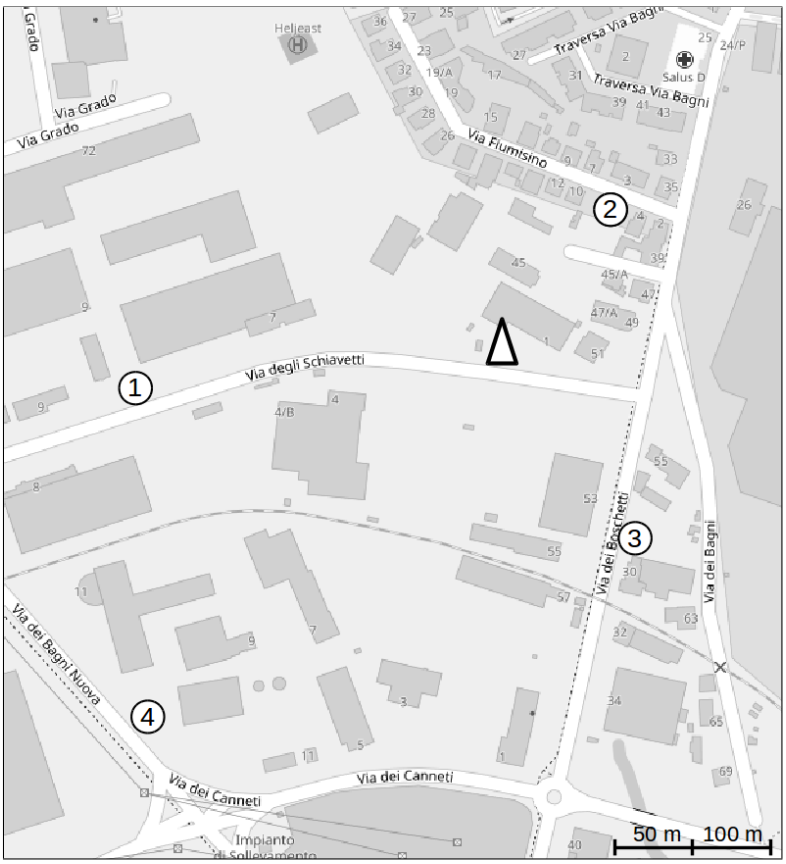

Figure 5.3: Map of the area where the measurements were performed. The triangle denotes the Base Station position, and the circles are the measurement positions. Map courtesy of OpenStreetMap Foundation [59].

arated by wide roads. The considered cellular mast carries 3 cell IDs for each operator arranged in a sectored configuration, and transmits on the 806 MHz and 816 MHz bands (LTE band 20), with a 10 MHz transmission bandwidth on both carrier frequencies. The measurements have been taken in four different positions around the location of the base station, as shown in Fig. 5.3. Positions 1 and 4 have a clear view of the transmitting antennas, while in positions 2 and 3 the mast is partially obscured by buildings and vegetation. Each measurement consists of 500 milliseconds of continuous recording. The

	Band 1	Band 2
Carrier Frequency [MHz]	806	816
Bandwidth [MHz]	10	10
$N_{\mathrm{RB}}^{\mathrm{DL}}$	50	50
Cell IDs	384,385,386	9,10,11
Antenna Ports	2	2
CP type	Normal	Normal

Table 5.1: Configuration of the considered base station.

instrumentation has been installed on a car for transportation, however the measurements were taken statically. The acquired data has been thoroughly searched for all visible Cell ID values, which have been compared to the values found within on-line archives [60] and those found with the use of the CellSearch [57] scan tool with the Elonics E4000 USB dongle. The identified cell IDs and other observed parameters for the 806 MHz band and the 816 MHz band are reported in Table 5.1.

6 Experimental Results

In this section, the proposed methods are applied to the real-life LTE data gathered during the measurement campaign. As it was done for the simulations, the range and standard deviation are used as metric to assess the performance of both methods when compared to single-band estimation. The results are discussed and tabulated for easier understanding.

6.1 Measurements Specifications

Each measurement consists of 500 milliseconds of continuous recording taken from a static position. This corresponds to 50 LTE downlink frames. However, as the measure is not synchronized with the frame structure of either transmitter, the number of full frames available in the recording will be less than 50. The transmitters are also not synchronized between each other, hence the CFR samples available for estimation do not span the whole 500 millisecond duration. Data is recorded with a sampling rate of 25 MSPS, which is down-sampled to 15.36 MHz in post-processing, corresponding to a FFT length of 1024. Each file contains the signal samples from both LTE transmitters, corresponding to 100 MB total of data. The measured data are first searched to infer the visible Cell IDs. For this purpose, the signal is correlated against a locally-generated CRS signal for all possible Cell ID values. This information is compared to the Cell ID values found within on-line archives and those found with the LTE Scan tool, and is needed to correctly extract the CFR using (1.12).

Similarly to the simulations, the $s = 0$ and $s = 4$ symbols of a slot are merged into a single symbol transmitted at $s = 0$ within the LTE slot. 20 consecutive symbols are grouped together, hence one ToA value is estimated for each LTE slot.

In the following sections the results derived from the measurements using both proposed methods are displayed. The ToA estimation results for each measure file are normalized, and the values of the chosen performance metrics are reported in the corresponding table.

In the measurement taken from Position 3, two cell IDs are visible in the 816 MHz band. Hence, two sets of estimations are shown for Position 3. On the other hand, the measurements taken in Position 2 did not produce any

significant result for the 806 MHz band. As such, results for Position 2 are not included.

6.2 Experimental Results - Signal Combining

The results obtained with the Signal Combining method are shown in Figs. 6.1-6.4. The displayed ToA values are normalized, as it was done for the simulated results, to unify the scale. Because the exact value of the ToA is not available, the estimations are normalized to the average value of dual-band estimation set. A table next to each figure summarizes the values of the range and standard deviation for the each set. The detected Cell IDs are reported as well. The CFR observed for both transmission bands presents a strong direct path, thanks to the clear view of the transmitter and the use of a directive antenna at the receiver. These conditions are ideal for the use of the Signal Combining method, which outperforms single-band estimation in all the considered cases.

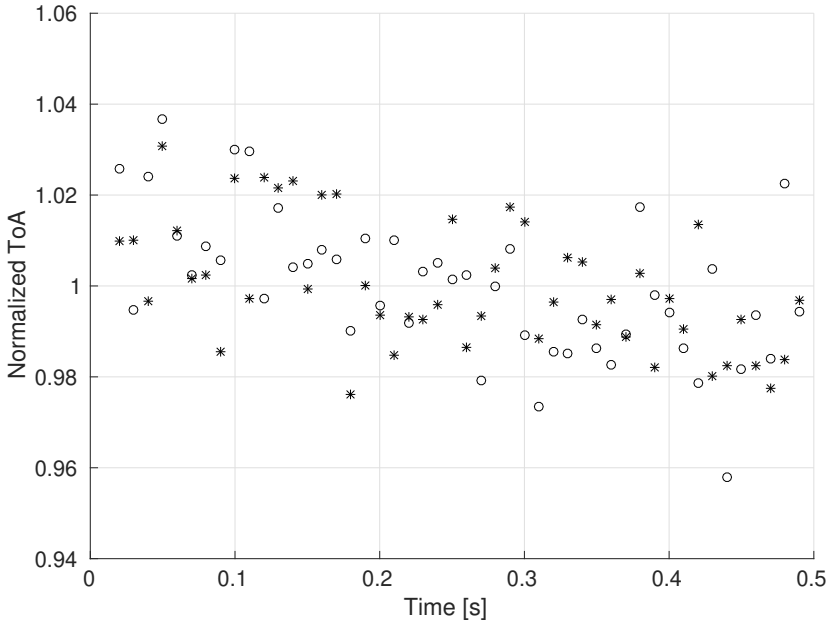

Figure 6.1: Normalized ToA estimation results using the Signal Combining method for Position 1 measurements. ∘: Single-band estimation ∗: Dual-band estimation.

Detected Cell IDs: 384, 10		
	Single-Band	Dual-Band Combining
r_τ [ns]	4.838	3.402
σ_τ [ns]	0.964	0.863

Table 6.1: ToA estimation results using the Signal Combining method for Position 1 measurements.

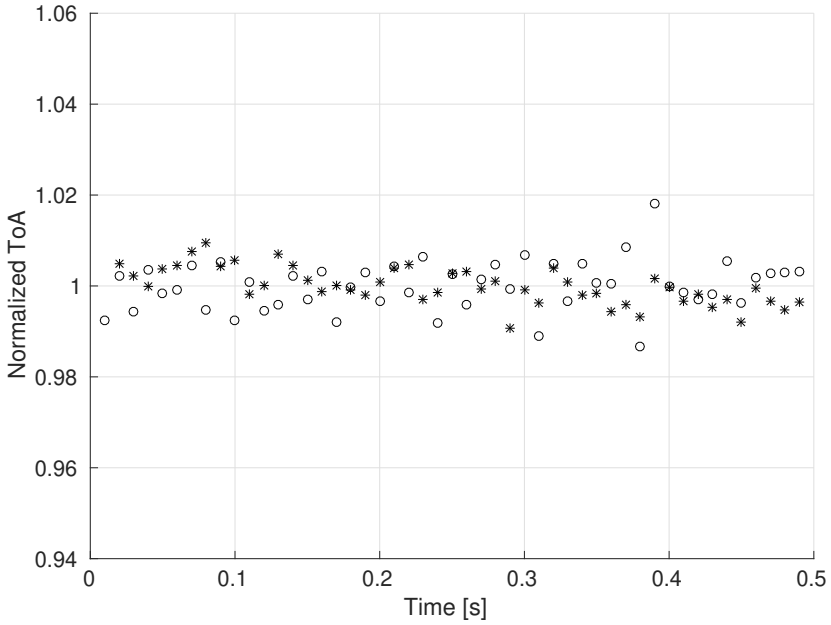

Figure 6.2: Normalized ToA estimation results using the Signal Combining method for Position 3 measurements (set 1). $\circ$: Single-band estimation $*$: Dual-band estimation.

Detected Cell IDs: 10, 386		
	Single-Band	Dual-Band Combining
r_τ [ns]	2.749	1.641
σ_τ [ns]	0.478	0.352

Table 6.2: ToA estimation results using the Signal Combining method for Position 3 measurements (set 1).

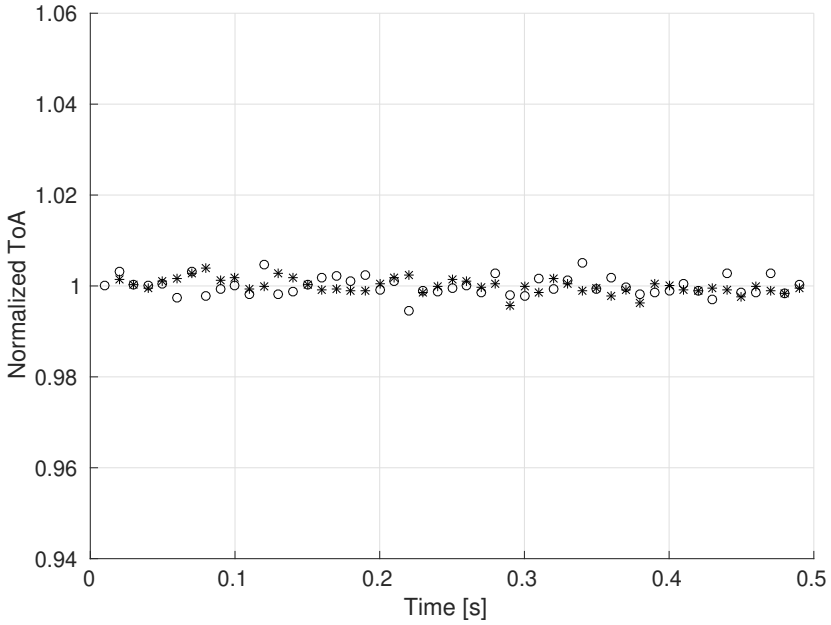

Figure 6.3: Normalized ToA estimation results using the Signal Combining method for Position 3 measurements (set 2). $\circ$: Single-band estimation $*$: Dual-band estimation.

Detected Cell IDs: 9, 386		
	Single-Band	Dual-Band Combining
r_τ [ns]	2.570	2.044
σ_τ [ns]	0.501	0.390

Table 6.3: ToA estimation results using the Signal Combining method for Position 3 measurements (set 2).

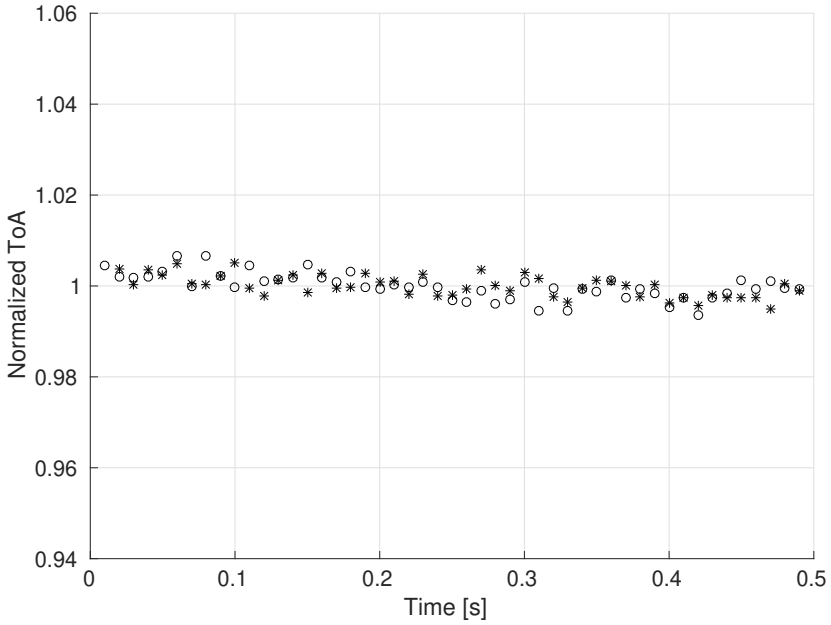

Figure 6.4: Normalized ToA estimation results using the Signal Combining method for Position 4 measurements. ∘: Single-band estimation ∗: Dual-band estimation.

Detected Cell IDs: 10, 386		
	Single-Band	Dual-Band Combining
r_τ [ns]	1.568	1.234
σ_τ [ns]	0.344	0.290

Table 6.4: ToA estimation results using the Signal Combining method for Position 4 measurements.

6.3 Experimental Results - Signal Aggregating

The results obtained with the Signal Aggregating method applied to real LTE data are shown in Figs. 6.5-6.8. Similarly to Signal Combining, the ToA values are normalized to the average value of the dual-band estimation set. Thanks to the favorable flat environment, Signal Aggregating achieves significant gain over single-band estimation. This is especially evident in Fig. 6.6, where the estimation obtained with the Signal Aggregating method shows a sharp decrease in both the performance metrics.

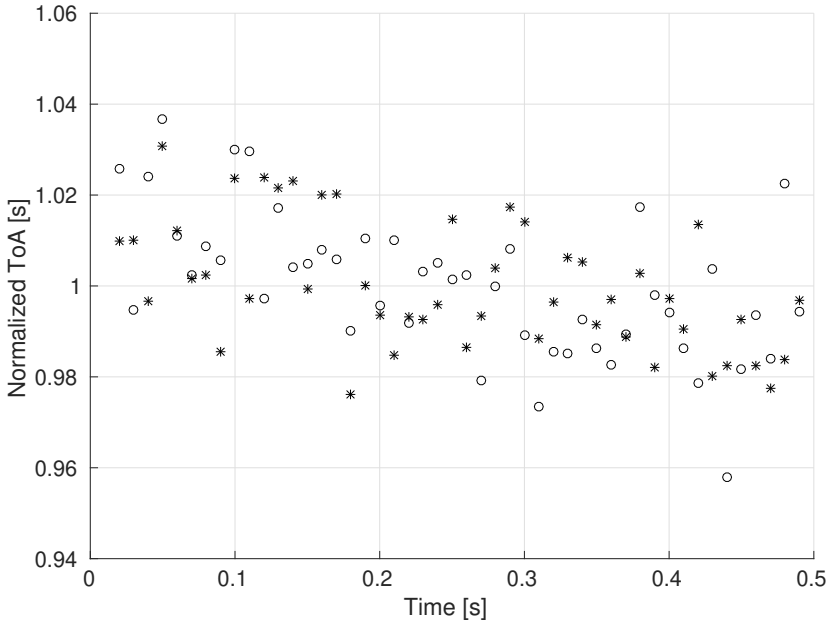

Figure 6.5: Normalized ToA estimation using the Signal Aggregating method for Position 1 measurements. ∘: Single-band estimation ∗: Dual-band estimation.

Detected Cell IDs: 10, 384		
	Single-Band	Dual-Band Aggregating
r_τ [ns]	4.838	2.083
σ_τ [ns]	0.964	0.341

Table 6.5: ToA estimation results using the Signal Aggregating method for Position 1 measurements (set 1).

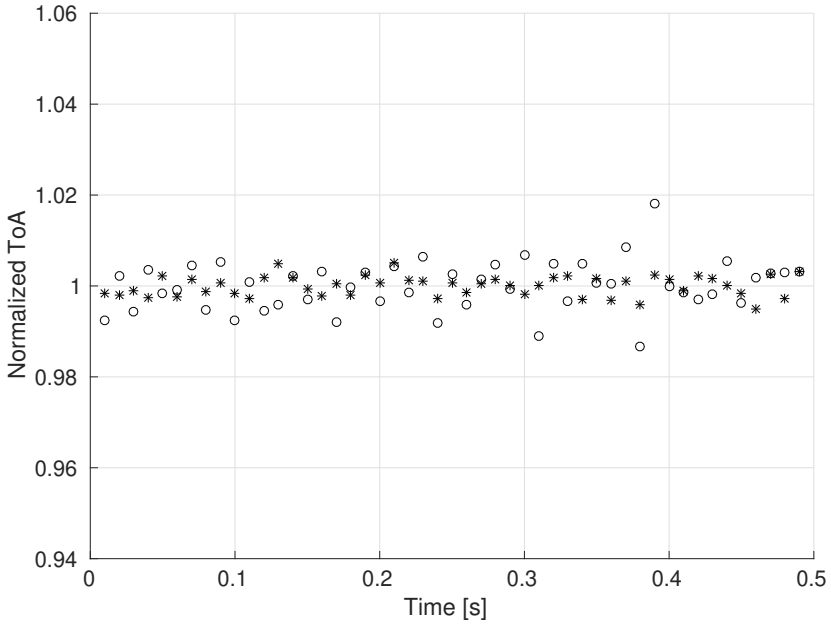

Figure 6.6: Normalized ToA estimation results using the Signal Aggregating method for Position 3 measurements (set 1). ∘: Single-band estimation ∗: Dual-band estimation.

Detected Cell IDs: 10, 386		
	Single-Band	Dual-Band Aggregating
r_τ [ns]	2.749	0.877
σ_τ [ns]	0.478	0.195

Table 6.6: Normalized ToA estimation results using the Signal Aggregating method for Position 3 measurements (set 2).

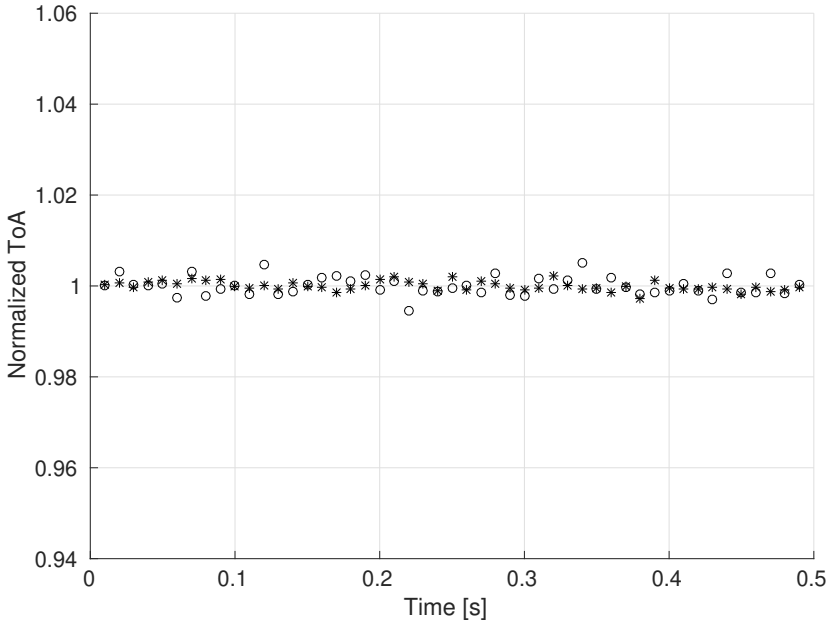

Figure 6.7: Normalized ToA estimation results using the Signal Aggregating method for Position 3 measurements (set 2). ∘: Single-band estimation ∗: Dual-band estimation.

Detected Cell IDs: 9, 386		
	Single-Band	Dual-Band Aggregating
r_τ [ns]	2.570	1.215
σ_τ [ns]	0.501	0.250

Table 6.7: ToA estimation results for Position 3 measurements using the Signal Aggregating method.

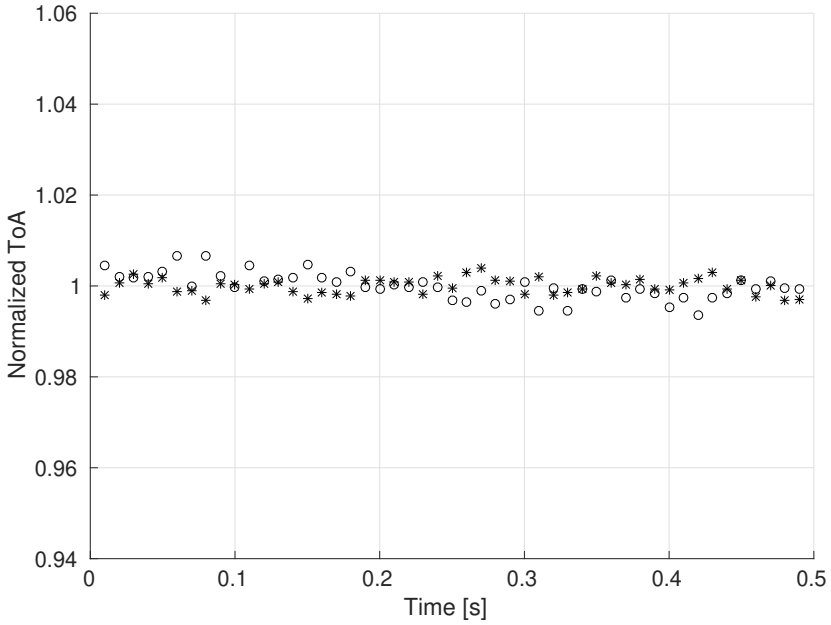

Figure 6.8: Normalized ToA estimation results using the Signal Aggregating method for Position 4 measurements. ∘: Single-band estimation ∗: Dual-band estimation.

Detected Cell IDs: 10, 386		
	Single-Band	Dual-Band Aggregating
r_τ [ns]	1.568	0.866
σ_τ [ns]	0.344	0.213

Table 6.8: ToA estimation results using the Signal Aggregating method for Position 4 measurements.

		Single-Band	Dual-Band Combining	Dual-Band Aggregating
Position 1	r_τ [ns]	4.838	3.402	2.083
	σ_τ [ns]	0.964	0.863	0.341
Position 3 (set 1)	r_τ [ns]	2.749	1.641	0.877
	σ_τ [ns]	0.478	0.352	0.195
Position 3 (set 2)	r_τ [ns]	2.570	2.044	1.215
	σ_τ [ns]	0.501	0.390	0.250
Position 4	r_τ [ns]	1.568	1.234	0.866
	σ_τ [ns]	0.344	0.290	0.213

Table 6.9: ToA estimation results.

6.4 Experimental Results - Summary

Both the Signal Combining and Signal Aggregating methods present better performance with respect to the chosen metrics (range and standard deviation) compared to single-band estimation, with Signal Aggregating generally achieving the best performance. This agrees with the results obtained from the simulation. Taking the measurement of Position 1 as an example, the range of the estimated ToA values decreases by 27.8% for Signal Combining and 61.2% for Signal Aggregating; the standard deviation decreases by 20.7% and 56.0% respectively for Signal Combining and Signal Aggregating. Similar results are observed from the data gathered in the other positions. In general, Signal Aggregating shows a larger performance gain when compared to Signal Combining. Table 6.9 summarizes the numerical results for comparison purposes.

7 Conclusions

This dissertation treated the problem of Time of Arrival estimation in OFDM systems, with a specific focus on the Third Generation Partnership Project (3GPP) Long Term Evolution (LTE) standard and on the possibility to combine multiple signals transmitted from the same physical mast on separate frequency bands. Among commercial standards, LTE standard stands out because of its high available bandwidth, comprehensive geographical coverage, and the physical properties of its downlink layer. The ToA information can be obtained opportunistically for positioning purposes. Indeed, it has been shown that the LTE standard can achieve good performance with regards to ranging accuracy [61].

Novel algorithms for the estimation of ToA in Orthogonal Frequency Division Multiplexing (OFDM) systems have been developed. The Slope-Based algorithm exploits the sub-carriers phase rotation, which presents a linear behavior, to estimate the ToA through a simple least-squares linear fitting procedure. The sub-carrier phase rotation can be easily estimated when bandwidth-spanning reference signals are present. This is a common occurrence in OFDM systems. When if the Direct Path (DP) is also the stronger one, the delay relative to the first path can be inferred from the slope of the phase rotation even in the presence of secondary paths. A piecewise variant of the alogrithm employs outliers removal to reduce the effects of noise and phase jumps on the final estimation. Piecewise linear fitting proves especially beneficial when the Signal to Noise ratio is low. The Slope-Based method is characterized by a low computational complexity, and achieves good performance when the direct path propagation is dominant.

In the Difference-Based ToA Estimation algorithm (DBTE) an estimate for the phase rotation frequency derivative is derived from the difference quo-

tient of the measured channel phase. A rough first estimate of the channel parameters is obtained by means of a simple FFT-based method. Using the inferred values, an estimation of the first propagation path delay can obtained even in the presence of strong secondary paths. The inaccuracies determined by noise are smoothed through the use of a sliding window average and an outliers removal procedure. Multiple consecutive symbols can be aggregated to achieve a more accurate and reliable estimate, giving the algorithm additional flexibility. The DBTE method achieves good performance at the cost of a greater computational complexity than the Slope-Based method.

Computer simulations have been used to validate the developed ToA estimation methods and assess their performance in a number of different propagation scenarios, using the Root Mean Square Error (RMSE) as the performance metric.

In the next part of the research work, the problem of multi-band ToA estimation has been researched. As the obtainable estimation accuracy is directly related to the available bandwidth [38, 39, 62], it becomes interesting to exploit multiple transmission bands at the same time, even when said bands are not contiguous. In the LTE network, base stations from multiple operators can be installed on the same physical station to realize better coverage, increased quality of service, and a reduction of deployment costs. This structure gives rise to a multi-band OFDM communication systems, where the transmission bands can be combined under the assumption that the propagation environment is flat across the whole bandwidth. This is often the case when the transmission bands are relatively close to each other.

The Space-Alternating Generalized Expectation-Maximization (SAGE) algorithm has been selected because of its versatility and good performance in complex propagation environments, without the need to change its basic

mathematical formulation. Initially introduced as an extension of Expectation-Maximization (EM) algorithm, it is a reduced complexity method for the evaluation of the Maximum Likelihood (ML) estimation. More precisely, in SAGE, the multi-dimensional ML estimation problem is subdivided into a certain number of smaller problems to jointly estimate the desired parameters in an iterative way. Efficient implementations of SAGE exist that can be easily adapted to estimate the parameters of interest, such as ToA [53], Doppler shift, and Angle of Arrival (AoA).

However, the general lack of synchronization between the clocks of the transmitters means that additional processing is needed before the information from the two sub-bands can be combined. To this end, two methods are introduced: Signal Combining and Signal Aggregating. Both methods employ phase shifting to match the input time-frequency matrices from each band to a common timebase. The time shift between the transmitters is first estimated and used to match the phases of the CFR sub-matrices. The time shift is assumed unchanging over the duration of several LTE frames.

In Signal Combining, the estimated Channel Frequency Responses (CFRs) from each sub-band are combined into a single matrix by means of the Maximal Ratio Combining (MRC) method. Signal Combining requires the reference signals for each transmission band to be analogous in their time-frequency structure, limiting it to scenarios where all the sub-systems are similarly structured and configured.

In Signal Aggregating, the channel samples matrices are instead joined into a larger matrix. Zero-filling is performed in the frequency gaps between sub-bands where no samples of the CFR are available. The zeros do not effect the outcome of the estimation and allow for a more efficient implementation of SAGE to be used. Signal Aggregating is more flexible with respect to the

sub-system structures and configuration. However, because of the largest size of the input matrix fed to the SAGE estimation algorithm, it is characterized by a greater computational cost than Signal Combining.

A simulator that accurately implements the LTE downlink layer has been developed to test and validate the band-combining methods. The Cell-Specific Reference Signal (CRS) has been used as the reference signal of choice, as it is always transmitted by the base station hence readily available for use. It has been shown that using the CRS for channel estimation purposes achieves the same performance as the dedicate Positioning Reference Signal (PRS) [62], encouraging its use in an opportunistic positioning framework. Both the Signal Combining and Signal Aggregating methods display interesting performance gain with respect to regular single-band estimation.

A set of live measurements on downlink LTE signals has been performed in Monfalcone, Italy. The instrumentation setup is based on two Software Defined Radio (SDR) devices, driven by an atomic reference clock to obtain synchronized sampling of separate frequency bands. The considered cellular mast carries 3 cell IDs for each operator, deployed in a sectored configuration, and transmits on LTE band 20. The Signal Combining and Signal Aggregating methods are compared to regular single-band estimation, using the range and standard deviation of the estimated delay values as performance indicators. The ToA is derived for the gathered data, showing (in agreement with simulations) that the combination of signals from multiple bands leads to a reduced range and standard deviation in the estimations. The Signal Aggregating method presents a greater performance gain compared to Signal Combining, at the cost of a slightly larger computational complexity.

The obtained numerical results are encouraging to explore more complex scenarios. Future works on the topic include testing the developed methods

in propagation environments characterized by stronger multi-path and user mobility. The possibility to combine signals of different nature, as technology develops toward denser and more integrated networks such as those expected in forthcoming fifth generation communication systems, becomes interesting as well. From a more theoretical standpoint, the bound on estimation accuracy for LTE signals in a complex propagation environment is a topic of interest, following the work of [62]. The methods for calculating the bound found in [39] are interesting, for they can be applied to any waveform and propagation channel specification.

References

[1] W.Dai, W. C. Lindsey, and M. Z. Win, "Accuracy of OFDM ranging systems in the presence of processing impairments," in *IEEE 17th International Conference on Ubiquitous Wireless Broadband*, Salamanca, Spain, September 2017.

[2] M. Z. Win and Y. Shen, "A theoretical foundation of network localization and navigation," *Proceedings of the IEEE*, vol. 106, 2018.

[3] F. Gustafsson and F. Gunnarsson, "Mobile positioning using wireless networks: possibilities and fundamental limitations based on available wireless network measurements," *IEEE Signal Processing Magazine*, vol. 22, July 2005.

[4] C. Gentner, S. Sand, and A. Dammann, "OFDM indoor positioning based on TDoA: Performance analysis and experimental results," in *International Conference on Localization and GNSS*, June 2012.

[5] C. Gentner and T. Jost, "Indoor positioning using time difference of arrival between multipath components," in *International Conference on Indoor Positioning and Indoor Navigation*, October 2013.

[6] A. Aasie-Ali, V. D. Nhuyen, K. Kyamakya, and A. S. Omar, "First arrival detection based on channel estimation for positioning in wireless OFDM systems," in *European Signal Processing Conference*, Florence, Italy, September 2006.

[7] A. Dammann, S. Sand, and R. Raulefs, "Signals of opportunity in mobile radio positioning," in *European Signal Processing Conference*, Bucharest, Romania, August 2012.

[8] ——, "On the benefit of observing signals of opportunity in mobile radio positioning," in *International ITG Conference on Systems, Communication and Coding*, Munich, Germany, June 2013.

[9] M. Driusso, F. Babich, F. Knutti, M. Sabathy, and C. Marshall, "Estimation and tracking of LTE signals time of arrival in a mobile multipath environment," in *IEEE International Symposium on Image and Signal Processing and Analysis (ISPA)*, Zagreb, Croatia, September 2015.

[10] M. Driusso, C. Marshall, M. Sabathy, F. Knutti, H. Mathis, and F. Babich, "Vehicular position tracking using LTE signals," *IEEE Transactions on Vehicular Technology*, vol. 66, no. 2, April 2017.

[11] K. Shamaei, J. Khalife, and Z. M. Massas, "Exploiting LTE signals for navigation: Theory to implementation," *IEEE Transactions on Wireless Communications*, vol. 17, no. 4, 2018.

[12] F. Benedetto, G. Giunta, and E. Guzzon, "Enhanced ToA-based indoor-positioning algorithm for mobile LTE cellular systems," in *Workshop on Positioning and Navigation and Communication*, Dresden, Germany, April 2011.

[13] N. Patwari, S. K. J. Ash, A. Hero, R. Moses, and N. Correal, "Cooperative localization in wireless networks," *IEEE Signal Processing Magazine*, vol. 22, 2005.

[14] H. Wymeersch, J. Lien, and M. Z. Win, "Locating the nodes: cooperative localization in wireless sensor networks," *Proceedings of the IEEE*, vol. 97, 2009.

[15] T. V. Nguyen, Y. Jeong, H. Shin, and M. Z. Win, "Least square cooperative localization," *IEEE Transactions on Vehicular Technology*, vol. 64, April 2015.

[16] L. Dai, Z. Wang, J. Wang, and Z. Yang, "Positioning with OFDM signals for the next-generation GNSS," *IEEE Transactions on Consumer Electronics*, vol. 56, no. 2, May 2010.

[17] Y.Chen, J. Peng, K. Huang, and X. Gong, "A multipath delay estimation model and algorithm in OFDM systems," in *IEEE International Conference on Communications (ICC)*, Kapaonik, Serbia, April-May 2002.

[18] M. Akdeniz, Y. Liu, M. Samimi, S. Sun, S. Rangan, T. Rappaport, and E. Erkip, "Millimeter wave channel modeling and cellular capacity evaluation," *EEE Journal on Selected Areas of Commununication*, vol. 32, June 2014.

[19] Y. G. Li and G. L. Stuber, *Orthogonal Frequency Division Multiplexing for Wireless Communications*. New York: Springer, 2006.

[20] L. Hanzo and T. Keller, *OFDM and MC-CDMA: A Primer*. Wiley-IEEE Press, 2006.

[21] B. Yang, K. Letaief, R. Cheng, and Z. Cao, "Channel estimation for OFDM transmission in multipath fading channels based on parametric channel modeling," *IEEE Transactions on Communications*, vol. 49, no. 3, March 2001.

[22] Y. Liu, Z. Tan, H. Hu, L. Cimini, and G. Li, "Channel estimation for OFDM," *IEEE Communications Surveys Tutorials*, vol. 16, no. 4, 2014.

[23] *Evolved Universal Terrestrial Radio Access (E-UTRA); Physical channels and modulation (Release 12)*, 3rd Generation Partnership Project, December 2015.

[24] *LTE Positioning Protocol*, 3rd Generation Partnership Project, April 2018.

[25] R. Zekavat and R. M. Buehrer, *Handbook of Position Location: Theory, Practice and Advances*. John Wiley & Sons, 2011.

[26] Y. Bar-Shalom, X. R. Li, and T. Kirubarajan, *Estimation with Applications to Tracking and Navigation: Theory Algorithms and Software*. John Wiley & Sons, 2011.

[27] E. D. Kaplan and C. J. Hegarty, *Understanding GPS, Principles and Applications*. Artech House, 2006.

[28] S. Mazuelas, A. Bahillo, R. M. Lorenzo, P. Fernandez, F. A. Lago, E. Garcia, J. Blas, and E. J. Abril, "Robust indoor positioning provided by real-time RSSI values in unmodified WLAN networks," *IEEE Journal on Selected Topics in Signal Processing*, vol. 3, October 2009.

[29] C. Yang and H. R. Shao, "Wifi-based indoor positioning," *IEEE Communications Magazine*, vol. 54, March 2015.

[30] B. Li, N. Wu, H. Wang, and J. Kuang, "Gaussian message passing for cooperative localization in wireless networks," in *IEEE/CIC International Conference on Communications in China*, Shanghai, China, October 2014.

[31] D. Dardari, E. Falletti, and M. Luise, *Satellite and Terrestrial Radio Positioning Techniques*. Elsevier, 2012.

[32] A. Z. Xu, E. Au, A. S. Wong, and Q. Wang, "A novel threshold-based coherent ToA estimation for IR-UWB systems," *IEEE Transactions on Vehicular Technology*, vol. 58, October 2009.

[33] G. L. Stuber, *Principles of Mobile Communication.* Boston: Kluwer Academic, 2001.

[34] X. Li, "RSS-based location estimation with unknown pathloss model," *IEEE Transactions on Wireless Communications*, vol. 5, December 2006.

[35] A. Giorgetti and M. Chiani, "Time-of-arrival estimation based on information theoretic criteria," *IEEE Transactions on Signal Processing*, vol. 61, no. 8, April 2013.

[36] J. Figueiras and S. Frattasi, *Mobile Positioning and Tracking. From Conventional to Cooperative Techniques.* Wiley, 2010.

[37] J. Pearl, "Reverend bayes on inference engines: A distributed hierarchical approach," in *National Conference on Artificial Intelligence*, Menlo Park, California, 1982.

[38] J. Ziv and M. Zakai, "Improved lower bounds on signal parameter estimation," *IEEE Transactions on Information Theory*, vol. 15, 1969.

[39] B. M. Sadler, N. Liu, and Z. Xu, "Ziv-Zakai bounds on time delay estimation in unknown convolutive random channels," *IEEE Transactions on Signal Processing*, vol. 58, May 2010.

[40] K. Thangarajah, R. Rashizadeh, S. Erfani, and M. Ahmadi, "A hybrid algorithm for range estimation in RFID systems," in *IEEE International*

Conference on Electronics and Circuits and Systems (ICECS), Ottawa, Canada, August 2012.

[41] M. Noschese, "September 2016 activities report," University of Trieste, Tech. Rep., September 2016.

[42] W. Li, X. Wang, and B. Moran, "Distance estimation using wrapped phase measurements in noise," *IEEE Transactions on Signal Processing*, vol. 61, no. 7, April 2013.

[43] X. Li, W. Wang, B. Yang, and Q. Yin, "Distance estimation based on phase detection with robust chinese remainder theorem," in *IEEE International Conference on Acoustic and Speech and Signal Processing (ICASSP)*, Florence, Italy, May 2014.

[44] Y. Chen, F. Wang, J. Wan, G. Li, and K. Xu, "An ambiguity-reduced phase unwrapping method and its applications in parameter estimation," in *IEEE International Conference on Signal Processing and Communications and Computing (ICSPCC)*, Ningbo, China, September 2015.

[45] F. Babich, M. Noschese, C. Marshall, and M. Driusso, "A simple method for ToA estimation in OFDM systems," in *IEEE European Navigation Conference (ENC)*, Lausanne, Switzerland, May 2017.

[46] "ALGLIB - C numerical analysis library." [Online]. Available: http://www.alglib.net/

[47] M. Patzold, *Mobile fading channels*. Wiley, 2002.

[48] T. Moon, "The expectation-maximization algorithm," *IEEE Signal Processing Magazine*, vol. 3, no. 6, November 1996.

[49] A. Dempster, N. Laird, and D. Rubin, "Maximum likelihood for incomplete data via the EM algorithm," *Journal of Royal Statistic Society Series B*, vol. 39, no. 1, 1977.

[50] G. McLachlan and T. Krishnan, *The EM Algorithm and Extensions*. New York: Springer, 1998.

[51] X. Li and K. Pahlavan, "Super-resolution ToA estimation with diversity for indoor geolocation," *IEEE Transactions on Wireless Communications*, vol. 3, no. 1, January 2004.

[52] E. Saberinia and A. H. Tefwik, "Ranging in multiband ultrawideband communication systems," *IEEE Transactions on Vehicular Technologies*, vol. 57, July 2008.

[53] H. Xu, C. C. Chong, I. Guvenc, F. Watanabe, and L. Yang, "High-resolution ToA estimation with multi-band OFDM UWB signals," in *IEEE International Conference on Communications*, Beijing, China, May 2008.

[54] B. Fleury, M. Tschudin, R. Heddergott, D. Dahlhaus, and K. I. Pedersen, "Channel parameter estimation in mobile radio environments using the SAGE algorithm," *IEEE Journal on Selected Areas of Communications*, vol. 17, no. 3, March 1999.

[55] C. C. Chong, D. I. Laurenson, C. M. Tan, S. McLaughlin, M. A. Beach, and A. R. Nix, "Joint detection estimation of directional channel parameters using the 2-D frequency domain SAGE algorithm with serial interference cancellation," in *IEEE International Conference on Information Science and Technology (ICIST)*, New York, USA, April 2014.

[56] J. A. del Peral-Rosado, J. A. López-Salcedo, G. Seco-Granados, P. Crosta, F. Zanier, and M. Crisci, "Downlink synchronization of LTE base stations for opportunistic ToA positioning," in *International Conference on Localization and GNSS*, Gothenburg, Sweden, June 2015.

[57] "LTE SDR cell scanner." [Online]. Available: https://github.com/Evrytania/LTE-Cell-Scanner

[58] "Ettus knowledge base." [Online]. Available: https://kb.ettus.com/Knowledge_Base

[59] "Openstreetmap." [Online]. Available: https://www.openstreetmap.org/

[60] "Cellular coverage and tower map." [Online]. Available: http://www.cellmapper.net

[61] J. D. Peral-Rosado, J. López-Salcedo, F. Zanier, and G. Seco-Granados, "Position accuracy of joint time-delay and channel estimators in LTE networks," *IEEE Access*, vol. 6, April 2018.

[62] M. Driusso, F. Babich, and C. Marshall, "Performance analysis of time of arrival estimation on OFDM signals," *IEEE Signal Processing Letters*, vol. 22, no. 7, July 2015.

Publications

Conference Papers

[1] F. Babich, F. Vatta and M. Noschese, "Analysis and Design of Rate Compatible LDPC Codes", International Symposium on Personal, Indoor, and Mobile Radio Communication (PIMRC), September 2016, Valencia, Spain.

[2] F. Babich, M. Noschese, C. Marshall and M. Driusso, "A simple method for TOA estimation in OFDM systems", European Navigation Conference (ENC), May 2017, Lausanne, Switzerland.

[3] M. Noschese, F. Babich, M. Comisso, C. Marshall and M. Driusso, "A Low-Complexity Approach for Time of Arrival Estimation in OFDM Systems", International Symposium on Wireless Communication Systems (ISWCS), August 2017, Bologna, Italy.

[4] F. Babich, F. Vatta, A. Soranzo and M. Noschese, "Low Complexity Rate Compatible Puncturing Patterns Design for LDPC Codes", International Conference on Software, Telecommunications and Computer Networks (SoftCOM), September 2017, Split, Croatia.

[5] M. Noschese, F. Babich, M. Comisso and C. Marshall, "On the Performance of SAGE Algorithm for ToA Estimation in Dual-Band OFDM Systems", International Symposium on Personal, Indoor, and Mobile Radio Communication (PIMRC), September 2018, Bologna, Italy.

Journal Papers

[1] F. Babich, F. Vatta, A. Soranzo and M. Noschese, "Low Complexity Rate Compatible Puncturing Patterns Design for LDPC Codes", Journal of Communications Software and Systems. Accepted November 2018.

Patents

[1] C. Marshall, A. Biason, M. Noschese, F. Babich, A. Pin and R. Rinaldo, "Estimating and using characteristic differences between wireless signals".